SAMPLES OF HOW TO INCLUDE PREVIOUSLY PUBLISHED ARTICLES AS CHAPTERS IN A THESIS OR DISSERTATION

by

The Thesis Office

The Thesis Office

The University of Utah

2014

This packet contains samples of how previously published articles should be included in a dissertation or thesis. Please note that any chapter that has not been published when beginning the format approval process will need to be formatted according to the University of Utah requirements. For additional information on formatting requirements, please consult A Handbook for Theses and Dissertations found on the Thesis Office website.

The first sample in this packet is from a document created in Word. Note the following for Chapter 2, the previously published chapter:

- The Table of Contents lists all the first-level subheadings in the previously published chapter, just as it does for the other unpublished chapters.
- The title of Chapter 2 is exactly the same as the published article's title.
- On the part-title page, there is a permission statement containing all pertinent information such as authors, article title, journal name, volume and page numbers where the article appeared.
- The page numbers for the dissertation appear in the top right corner; that is, the pages on which the previously published article has been inserted into the dissertation are still numbered consecutively with the rest of the dissertation pages.
- The article fits within the 1 ¼" side margins and 1" top and bottom margins.

TABLE OF CONTENTS

CHAPTER 2

PHYLOGENETIC RELATIONSHIPS IN *SOLANUM* SECTION *ANDROCERAS* (SOLANACEAE)

Reprinted with permission from Stern, S., Weese, T. and Bohs, L. 2010. Phylogenetic Relationships in *Solanum* Section *Androceras* (Solanaceae), *Systematic Botany* 35: 885-893.

Systematic Botany (2010), 35(4): pp. 885–895
© Copyright 2010 by the American Society of Plant Taxonomists
DOI: 10.1600/036364410X539934

Phylogenetic Relationships in *Solanum* Section *Androceras* (Solanaceae)

Stephen R. Stern,[1] Terri Weese,[1] and Lynn A. Bohs[1,2]

[1]Department of Biology, University of Utah, 257 South 1400 East, Salt Lake City, Utah 84112-0840, U. S. A.
[2]Author for correspondence (bohs@biology.utah.edu)

Communicating Editor: Anne Bruneau

Abstract—The Leptostemonum clade of *Solanum* contains approximately 350–450 species, including the cultivated eggplant, *S. melongena*. This clade is characterized by the presence of prickles and apically attenuate anthers. *Solanum* section *Androceras*, the focus of this study, is a group of ca. 12 species belonging to the Leptostemonum clade. This section is unusual in the genus because of its mostly north temperate distribution and distinctive zygomorphic, heteranatherous, and enantiostylous flowers. We infer phylogenetic relationships among 43 *Solanum* taxa, including 11 species and all varieties of sect. *Androceras*, using DNA sequence data from two nuclear regions (ITS and the granule-bound starch synthase gene [GBSSI or *waxy*]) and the chloroplast region *trnT-F*. The combined phylogenetic tree supports sect. *Androceras* as a monophyletic group sister to *Solanum* sect. *Crinitum*. Only one of the three series proposed by previous taxonomists, ser. *Pacificum*, is supported as monophyletic. *Solanum tenuipes* from the northern Chihuahua Desert is sister to the remaining species in sect. *Androceras*. Species-level relationships were also examined and it was found that two species, *S. heterodoxum* and *S. citrullifolium*, are not monophyletic. The ancestral flower color in sect. *Androceras* appears to be violet, with white and yellow flowers restricted to more derived clades. Characters formerly used to diagnose ser. *Androceras*, such as exclusively branched hairs and lack of complex foliar flavonoids, appear to have evolved more than once in the section.

Keywords—enantiostyly, heteranthery, ITS, Mexico, *trnT-F*, *waxy*.

Solanum L. (Solanaceae), thought to contain approximately 1,400 species, is one of the 10 largest genera of flowering plants (Frodin 2004; Bohs 2005). It also contains economically important species such as the tomato (*S. lycopersicum* L.), eggplant (*S. melongena* L.), and potato (*S. tuberosum* L.). Recent studies of the genus range from sequencing the genome of the tomato (Mueller et al. 2005; http://www.sgn.cornell.edu/) to resolving phylogenetic relationships within *Solanum* as well as species level taxonomy (Knapp et al. 2004; http://www.nhm.ac.uk/solanaceaesource/). With respect to the phylogeny of the genus, analyses of DNA sequence data have helped to identify the major groups within *Solanum*, the largest of which is the Leptostemonum clade with approximately 350–450 species (Bohs 2005; Levin et al. 2006). This group is commonly known as the "spiny solanums" due to the presence of sharp epidermal prickles.

Within the Leptostemonum clade, *Solanum* sect. *Androceras* is unique in many features including distribution, flower and fruit morphology, and chemistry. Its morphological characteristics, specifically floral morphology, are so distinct that Nuttall (1818) placed the species in the genus *Androcera* Nutt., although he noted the similarities between *Androcera* and *Solanum*. Marzell (1927) placed the species of *Androcera* into *Solanum* sect. *Androceras*. Whalen (1979a) provided a detailed revision of *Solanum* sect. *Androceras*, including 12 species and 10 varieties, and divided the section into three series (discussed below; Table 1) based on hair, flower, seed, and chemical characteristics as well as geographical distributions. Species in the section range from the midwestern U. S. A. through Mexico to Honduras, with the highlands around Mexico City, the northern Chihuahuan Desert, and the west coast of Mexico as centers of diversity (Table 1). This section is one of the only groups in *Solanum* to have a primarily north temperate distribution. Within its range, species of sect. *Androceras* are weedy annual herbs or perennials from persistent woody roots. Many species grow in warm, semiarid to arid regions with unpredictable seasonal rainfall. Chromosome counts have been reported for all species in sect. *Androceras*, and all are diploids with $2n = 24$ (Whalen 1979a).

Typical *Solanum* flowers are radially symmetrical with stamens dehiscing by terminal pores. They are usually buzz pollinated, ejecting pollen from the pores when vibrated by bees. Species in sect. *Androceras* conform to this basic plan, but are further specialized in being bilaterally symmetrical. The stamens within a single flower are unequal in size, with four small, straight upper anthers and an elongate lower anther (heteranthery; Bohs et al. 2007). This elongated, inwardly-curved lowermost stamen can be a different color than the other stamens and is opposed by a slender style of similar shape (Fig. 1a, b, c). The position of the style alternates between the right and left side of the flower along the inflorescence, resulting in "mirror-image" flowers (enantiostyly).

Flowers of sect. *Androceras*, specifically *S. rostratum*, have been extensively observed in field and natural history studies with a focus on the unusual stamen dimorphism (Todd 1882; Harris and Kuchs 1902; Bowers 1975; Jesson and Barrett 2002). The upper four small stamens provide the pollen that the bees use for food, whereas the lowermost, elongated stamen acts as a pollinating stamen by depositing pollen on one side of the bee's abdomen where it cannot efficiently be removed (Bowers 1975; Vallejo-Marin et al. 2009). The alternating right- and left-handed flowers have been shown to have higher outcrossing rates than plants manipulated to have either straight styles or right-handed or left-handed flowers only (Jesson and Barrett 2002). This might be especially important in maintaining genetic diversity in sect. *Androceras*, where all tested species have been found to be self-compatible (Whalen 1979a).

Most species of *Solanum* have fleshy berries, whereas fruits in sect. *Androceras* are dry at maturity and tightly enveloped by a prickly, accrescent calyx (Fig. 1d). Whalen (1979a) showed that these represent a "censer" dispersal mechanism, also seen in other members of the Leptostemonum clade, particularly those of dry habitats, in which the fruits remain on the plant and the calyx splits open, tearing the dry berry (Symon 1984; Knapp 2002). This then acts like a "censer," shaking loose the small seeds. The large number of seeds produced by a single plant, in some cases over 5,000 seeds from an individual, corresponds to the observation that *Solanum* sect. *Androceras* is typically a weedy, colonizing group of species.

Some species of sect. *Androceras* have a unique suite of flavonoid compounds, such as 8-hydroxyflavonoids and C-glycosylflavones, not found in other *Solanum* groups (Whalen 1978a). Differences also exist in the chemical profiles between the three series within the section recognized

TABLE 1. Species of *Solanum* sect. *Androceras*, including the series and their distributions according to Whalen (1979a). All taxa except *S. leucandrum* were sampled in this study.

Solanum section *Androceras* (Null) Marzell	Geographic Distributions
Series *Androceras*	
S. angustifolium Mill	Tropical Mexico south to Honduras
S. fructo-fecto Cav.	Distrito Federal, Hidalgo, and México States with collections from Ciudad Durango and the Sierra Madre, Mexico
S. johnstonii Whalen	Endemic to eastern Durango State, Mexico
S. rostratum Dunal	Widespread from Mexico City through the Great Plains, U.S.A.; introduced worldwide
S. tribulosum Schauer	Querétaro to southeastern Puebla State, Mexico
Series *Pacificum* Whalen	
S. grayi Rose var. *grayi*	Southern Sonora and northern Sinaloa, Mexico
var. *grandiflorum* Whalen	Southern Sinaloa and south along the Sierra Madre, east to Guerrero inland in central Mexico to Morelos
S. leucandrum Whalen	Known only from the type locality in western Puebla, Mexico
S. lumholtzianum Bartlett	Southern Arizona, and Sonora to northern Sinaloa, Mexico
Series *Violaceiflorum* Whalen	
S. citrullifolium A. Braun var. *citrullifolium*	North-central Coahuila, Mexico to the Davis Mts. of western Texas, with a cluster of populations in central Texas
var. *knoblochii* Whalen	Known only from two localities in Tarahumara country of western Chihuahua, Mexico
var. *setigerum* Bartlett	Eastern Chihuahua and western Coahuila, occasionally Presidio County, Texas
S. daviesiae Whalen	Davis, Chinati, and Chisos Mts. of west Texas and Sierra del Carmen in northern Coahuila, Mexico
S. heterodoxum Dunal var. *heterodoxum*	Veracruz northwest across Puebla and Hidalgo to San Luis Potosí, Mexico
var. *novomexicanum* Bartlett	Mountains of north-central New Mexico
var. *setigerodes* Whalen	Northern Chihuahua, southeastern Arizona, and southwestern New Mexico
S. tenuipes Bartlett var. *tenuipes*	Eastern Coahuila State, Mexico to Brewster, Terrel, Val Verde, and Maverick Counties, Texas
var. *latisectum* Whalen	Presidio County, Texas south along the Chihuahua and Coahuila borders to eastern Durango, Mexico

by Whalen (1979a), such as the presence of methoxylated aglycones, 8-hydroxyflavonoids and various flavones in sers. *Violaceiflorum* and *Pacificum* that are absent in ser. *Androceras*. The major chemical differences between sers. *Violaceiflorum* and *Pacificum* are flavones with chrysoeriol type B-rings in ser. *Pacificum* and the presence of 8-oxygenated flavonols in ser. *Violaceiflorum* (Whalen 1978a).

Although Whalen (1979a) revised sect. *Androceras* and included a cladistic analysis based on 14 morphological and chemical traits, to date there have been limited molecular phylogenetic studies of this section. Two species of sect. *Androceras*, *S. rostratum* and *S. citrullifolium*, were included in molecular phylogenies of the entire Leptostemonum clade and were strongly supported as sister taxa (Levin et al. 2006; Bohs et al. 2007). These studies place sect. *Androceras* sister to sect. *Crinitum* Child with moderate support (84% bootstrap and 1.0 posterior probability in Levin et al. 2006). This relationship had not previously been proposed due to the fact that sect. *Crinitum* is a South American group of large shrubs and trees with fruits that may reach 10 cm in diameter and large flowers that are not heterantherous. A close relationship between sect. *Androceras* and *S. sisymbriifolium* of sect. *Cryptocarpum* Dunal has been proposed in the past due to their similar leaves, inflorescences, and accrescent calyces (Dunal 1813, 1852; Walpers 1844; Danert 1970; Whalen 1979a; Lester et al. 1986). Both Weese and Bohs (2007) and Bohs et al. (2007) have found that *S. sisymbriifolium* is sister to a clade composed of sect. *Androceras* and sect. *Crinitum*. Whalen (1979a) favored sect. *Nycterium* (Venten.) Walp. as the sister group to sect. *Androceras* based on morphological similarities, but molecular studies unequivocally place the members of sect. *Nycterium* quite distant from sect. *Androceras* (Levin et al. 2006; Bohs et al. 2007; Weese and Bohs 2007). While these studies provide hypotheses about relationships between sect. *Androceras* and other *Solanum* sections, they did not extensively sample from within the section.

In this paper we use molecular phylogenetic methods to 1) test the monophyly of sect. *Androceras* as currently circumscribed, 2) examine the phylogenetic relationships of sect. *Androceras* with closely related members of the Leptostemonum clade, 3) test the monophyly of Whalen's (1979a) series and species within sect. *Androceras*, and 4) examine selected species-level relationships to test hypotheses of character evolution and speciation proposed by Whalen (1979a).

MATERIALS AND METHODS

Taxon Sampling—Eleven of the 12 species and all 10 varieties in sect. *Androceras* sensu Whalen (1979a) were sampled for this study (Table 1). We were unable to obtain high quality genomic DNA for *Solanum leucandrum*, which is known only from the type locality in Puebla, Mexico, due to a lack of available herbarium material. Specimens were determined using keys found in Whalen (1979a), with almost half of the specimens determined by the late Michael D. Whalen himself (indicated with asterisks in Appendix 1). We also included six members of sect. *Crinitum* as well as *S. sisymbriifolium*, both shown by previous molecular studies to be closely related to sect. *Androceras* (Levin et al. 2006; Bohs et al. 2007). Five other more distantly related species from the Acanthophora and Bahamense clades of the Leptostemonum clade were included to ensure sufficient outgroup sampling, and the tree was rooted using *S. betaceum*, an even more distantly related *Solanum* from outside the Leptostemonum clade. The final data set included 43 accessions, representing 11 named species of sect. *Androceras* as well as 12 outgroup species. All taxa, along with voucher information and GenBank accession numbers, are listed in Appendix 1.

DNA Extraction, Amplification, and Sequencing—Total genomic DNA was extracted from fresh, silica gel-dried, or herbarium material using the DNeasy plant mini extraction kit (Qiagen, Inc., Valencia, California). Amplification for each gene region followed standard procedures described in Taberlet et al. (1991), Bohs and Olmstead (2001), and Bohs (2004) for the *trnT-L* and *trnL-F* intergeneric spacer regions; Levin et al. (2005) for *waxy*, and Levin et al. (2006) for ITS. The ITS region was amplified as a single fragment using primers ITSleu1 (Bohs and Olmstead 2001) and ITS4 (White et al. 1990) using PCR conditions described in Bohs and Olmstead (2001). When possible, *trnT-F* and *waxy* were amplified as single fragments using primers a and f for *trnT-F* (Taberlet et al. 1991) and primers waxyF and waxy2R for *waxy* (Levin et al. 2005). Amplification conditions for *trnT-F* followed Bohs and Olmstead (2001); conditions for *waxy* followed Levin et al. (2005). When necessary, overlapping fragments were amplified and assembled, using primers a with d, and e with f to amplify *trnT-F*, and primers waxyF with 1171R, and 1058F with 2R to amplify *waxy*. Specimens not amplifying for *waxy* were amplified in

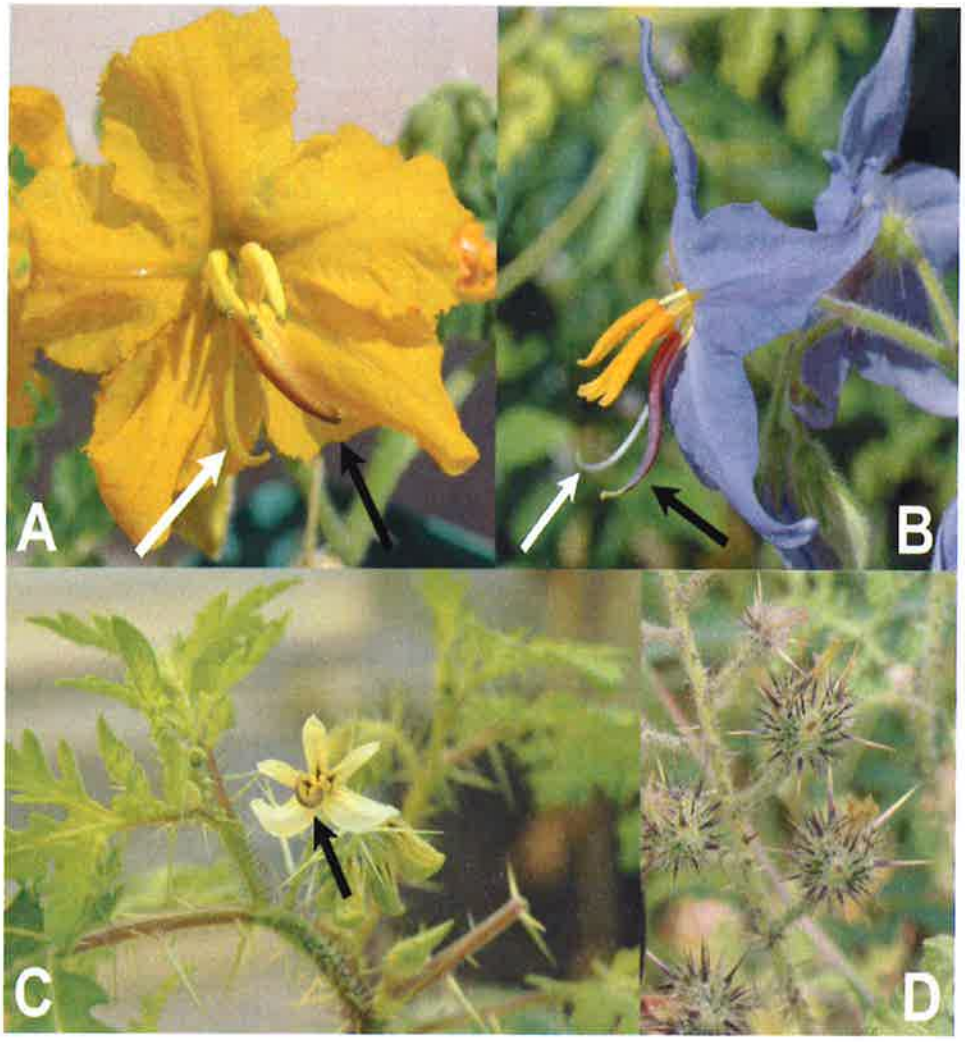

FIG. 1. Representatives of *Solanum* sect. *Androceras*. White arrows indicate the style and black arrows indicate the enlarged lower anther. A. *S. rostratum* of Whalen's ser. *Androceras* and our Rostratum clade. B. *S. citrullifolium* var. *citrullifolium* of Whalen's ser. *Violaceiflorum* and our Sehigeroid clade. C. *S. grayi* var. *grandiflorum* of Whalen's ser. *Pacificum* and our Pacificum clade. D. Typical fruits of sect. *Androceras* from *S. rostratum*. Photos C, D courtesy of M. Vallejo-Marin.

even smaller fragments using primers waxyF and the newly developed EX3R (5′-CACAACCTGAACCTAAG-3′) for the first fragment, the new primer EX4F (5′-CTATGGCCCCAAAGCTGGAC-3′) and 1171R for the second fragment, primers 1058F and 3′N (Peralta and Spooner 2001) for the third fragment, and primers 3′F (Miller et al. 1999) and 2R for the final fragment.

Amplification products were cleaned using the Promega Wizard SV PCR Clean-Up System (Promega Corporation, Madison, Wisconsin). The University of Utah DNA Sequencing Core Facility performed sequencing on an ABI automated sequencer. Sequences were edited in Sequencher (Gene Codes Corp., Ann Arbor, Michigan) and all new sequences were submitted to GenBank.

Morphological Data—The data matrix presented in Whalen (1979a; Table 6), representing 11 morphological, two chemical, and one isozyme character for species in sect. *Androceras* was added to the combined molecular data matrix with characters for outgroup species coded as missing data.

Sequence Alignment and Analysis—Sequence alignment for all gene regions was straightforward and performed visually using Se-Al (Rambaut 1996). The aligned datasets and representative phylogenetic trees are available in TreeBASE (study number S2642).

Parsimony Analyses—Maximum parsimony (MP) analyses were performed on each dataset separately and on the combined dataset both with and without morphological data using PAUP*4.0b10 (Swofford 2002). All characters were weighted equally in analyses that implemented tree bisection reconnection (TBR) branch swapping with 1,000 heuristic random addition replicates, each limited to 1,000,000 swaps per replicate. Gaps were treated as missing data. Bootstrapping (BS, Felsenstein 1985) was used to evaluate branch support with 1,000 random addition replicates and TBR branch swapping limited to 1,000,000 swaps per replicate. Datasets were further analyzed using TNT (Goloboff et al. 2008) to search for shorter trees than were obtained in standard PAUP analyses. Congruence of the datasets was tested using partition homogeneity tests (incongruence length difference test [ILD]; Farris et al. 1994, 1995)

implemented in PAUP*. One thousand heuristic partition homogeneity replicates were completed, each with 10 random addition sequence replicates, TBR branch-swapping, MulTrees off, and gaps treated as missing data.

Bayesian Analyses—Prior to Bayesian analyses (BI), a general model of nucleotide evolution was selected for each of the separate and combined datasets using the AIC criterion identified in Modeltest 3.7 (Posada and Crandall 1998). MrBayes 3.1 (Huelsenbeck and Ronquist 2001) was used to analyze the individual and combined datasets. For each analysis 20 replicates were run of four Markov chains, each initiated from a random tree and sampled every 1,000 generations using the stop rule to stop the analysis when standard deviations between the runs reached 0.01. All parameters from each analysis were visualized graphically and the samples obtained prior to achieving stationarity were discarded as a burn-in.

Constraint Analyses—Constraint trees were constructed in MacClade 4 (Maddison and Maddison 2000) to constrain 1) each of Whalen's (1979a) series as monophyletic, 2) only the taxa in ser. *Androceras* as monophyletic, 3) only the taxa in ser. *Violaciflorum* as monophyletic, and 4) the yellow-flowered taxa as monophyletic. Parsimony analyses were performed with the constraint enforced using TBR branch swapping with 1,000 heuristic random addition replicates, each limited to 1,000,000 swaps per replicate. These trees were then compared with the most parsimonious trees using the Templeton test (Templeton 1983; Prager and Wilson 1988).

Results

Phylogenetic Analyses—Descriptive statistics for the molecular datasets and phylogenetic analyses for the 43 accessions are given in Table 2. Missing data comprised 0.00087% of the combined data matrix (149 bases from a total of 171,907). For the individual datasets, the *trnT-F* region yielded the least resolved phylogeny in both MP and BI analyses. The *waxy* data produced the most resolved trees with the highest number of strongly supported ingroup nodes (Table 2). In general, the parsimony strict consensus and BI majority rule consensus trees from the combined dataset differed only in the degree of resolution, with BI tree topologies more resolved than parsimony trees (Table 2). Clades with low posterior probabilities (PP) in BI analyses were often collapsed in MP strict consensus trees (individual trees not shown).

More nodes were strongly supported by combining the three datasets than were obtained in any of the separate analyses (Table 2; Fig. 2). Inclusion of morphological data did not affect either the topology or resolution of the phylogeny compared to the combined molecular dataset analyzed alone. The only differences between these and the strictly molecular trees were slight differences in support values for a few nodes.

Topological Conflicts—According to the results of the ILD tests, the three data partitions in the combined data set were found to be incongruent ($p = 0.033$), so pairwise ILD tests were run. The nuclear datasets (ITS and *waxy*) were found to be incongruent ($p = 0.01$) as were the *waxy* and *trnT-F* datasets ($p = 0.01$). The only congruent datasets were ITS and *trnT-F* ($p = 0.071$). The incongruence of the datasets is likely due to the disparity in the size and substitution rates of the different datasets (Dolphin et al. 2000; Barker and Lutzoni 2002; Darlu and Lecointre 2002). However, with few exceptions, each DNA sequence region consistently identified the same major, well-supported clades comprising identical species groups, but relationships among clades were often not strongly supported (BS values < 90%), or were unresolved, and thus cannot be considered conflicting under Wiens' (1998) criteria. The BI analysis gave more conflicting nodes (cutoff at < 0.95 PP), but posterior probabilities are known to be inflated relative to bootstrap values (Cummings et al. 2003; Erixon et al. 2003; Simmons et al. 2004). Our discussion will be focused on the topology of the BI majority rule and MP strict consensus trees based on combined molecular data (Fig. 2).

Phylogenetic Relationships—Sectional Relationships and Monophyly of Section *Androceras*—All data sets strongly support the monophyly of sect. *Androceras* as circumscribed by Whalen (1979a, 1984; 100% BS, 1.0 PP in ITS, *waxy* and combined gene trees and 99% BS, 1.0 PP in *trnT-F*).

Although not supported in the single-gene analyses, the combined dataset supports sect. *Crinitum* as sister to sect. *Androceras* (88% BS, 1.0 PP), with *Solanum sisymbriifolium* sister to the clade composed of sects. *Androceras* and *Crinitum* (85% BS, 1.0 PP).

Monophyly of the Series Within Section *Androceras*—Of the three series identified by Whalen (1979a), our phylogeny supports only ser. *Pacificum* as a monophyletic group, termed the Pacificum clade in Fig. 2. This relationship is supported in the individual ITS (87% BS, 1.0 PP) and *waxy* (98% BS, 1.0 PP) but not in the *trnT-F* dataset; the combined dataset resolves this group with 100% BS and 1.0 PP. Three of the five species of ser. *Androceras* form a moderately to strongly supported Rostratum clade composed of *S. rostratum*, *S. fructotecto*, and *S. angustifolium* in the *waxy* only (82% BS, 1.0 PP) and combined trees (94% BS, 1.0 PP). *Solanum johnstonii* of ser. *Androceras* is unplaced in the ITS, *trnT-F*, and combined analyses; the *waxy* only analysis places this species as sister to the Pacificum clade with moderate support (86% BS, 1.0 PP). The final member of Whalen's ser. *Androceras*, *S. tribulosum*, is moderately supported (82% BS, 1.0 PP) as sister to a large clade of species, placed by Whalen (1979a) in ser. *Violaciflorum*, in the combined analyses, but this relationship is not recovered in any of the individual analyses. Whalen's ser. *Violaciflorum* is clearly polyphyletic, with a large clade composed of *S. heterodoxum* var. *setigeroides*, *S. citrullifolium* vars. *citrullifolium* and *setigerum*, and *S. dulcisense* forming a monophyletic group, here termed the Setigeroid clade, in the *waxy* only (90% BS, 1.0 PP) and combined analyses (92% BS, 1.0 PP; Fig. 2). The remainder of the taxa belonging to Whalen's ser. *Violaciflorum*, including *S. lennipes*, *S. citrullifolium* var. *knobhchii*, and *S. heterodoxum* vars. *heterodoxum* and *novomexicanum* form a grade at the base of the Androceras clade in the combined analyses. "Elder 46", a potentially undescribed

Table 2. Descriptive statistics for the datasets analyzed. Strongly supported nodes for parsimony indicate those with ≥ 90% BS; Bayesian strongly supported nodes are those with ≥ 0.95 PP.

Data Partition	Aligned Sequence Length	Number of Parsimony Informative Characters	Number of MP Trees	Tree Length	CI	RI	Number of Strongly Supported Nodes: Parsimony (ingroup nodes)	Model Selected	Number of Strongly Supported Nodes: Bayesian (ingroup nodes)
ITS	666	121	13,691	431	0.608	0.783	11 (6)	GTR + I + G	21 (15)
waxy	1,731	165	48	428	0.844	0.895	17 (12)	GTR + G	32 (24)
trnT-F	2,088	65	52,750	188	0.910	0.895	6 (3)	GTR + I + G	13 (8)
Combined	4,485	340	10	1,085	0.733	0.829	18 (12)	GTR	36 (24)
Combined + Morphological	4,490	354	6	1,127	0.726	0.828	16 (12)	GTR	38 (27)

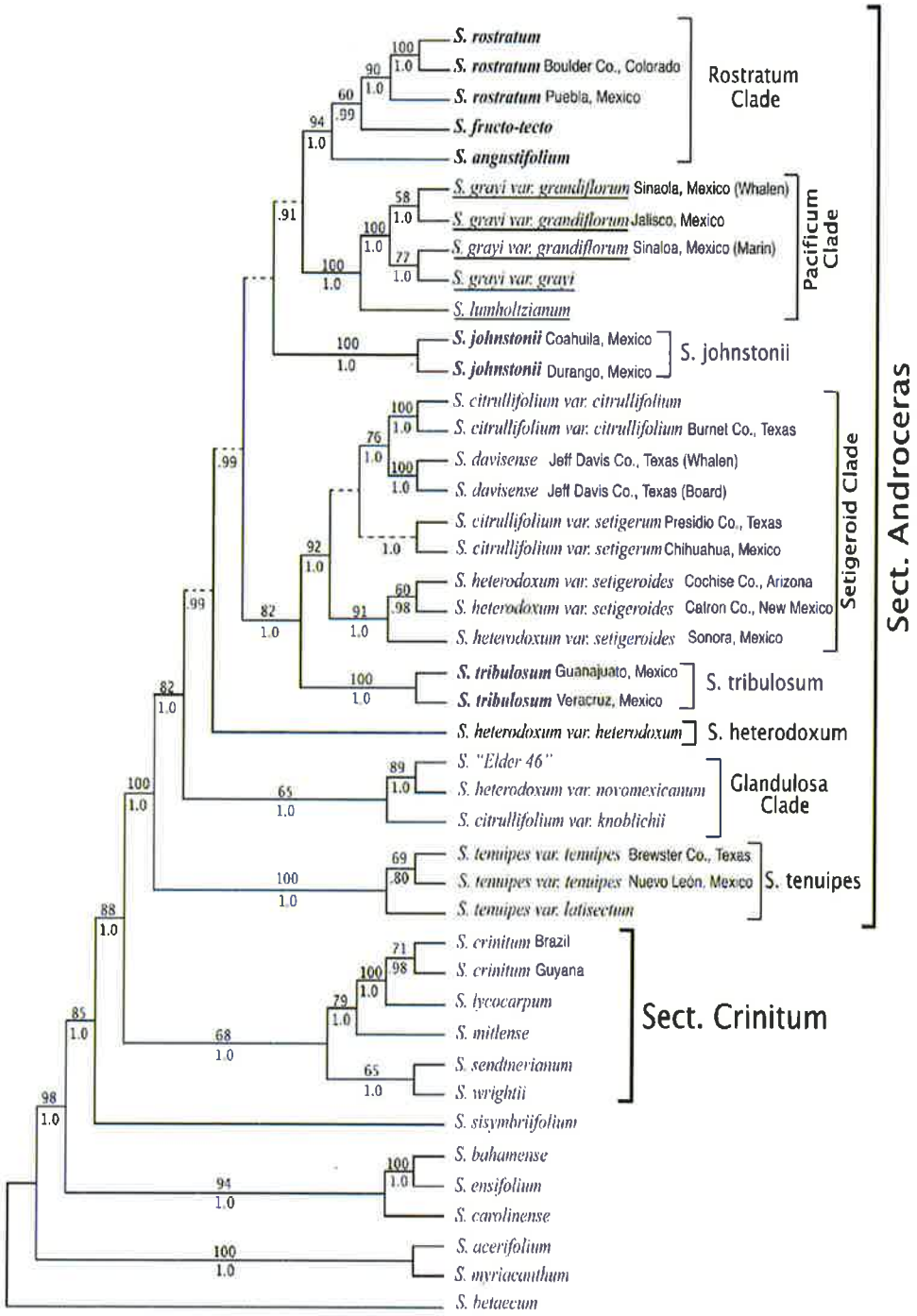

FIG. 2. 50% majority rule tree from the Bayesian analysis of the combined dataset. Numbers above branches are bootstrap values over 50%, numbers below branches are posterior probabilities from Bayesian analysis. Branches that collapse in the parsimony strict consensus tree but are present in the Bayesian majority rule tree are shown as dashed lines. Species of sect. *Androceras* placed by Whalen (1979a) in ser. *Androceras* are in bold italics, in ser. *Pacificum* are underlined, and in ser. *Violaceiflorum* are in nonbold italics. *Solanum* "Elder 46" was not placed in any of Whalen's (1979a) series; see text for discussion. The clades discussed in the text are labeled.

species, is strongly supported as sister to *S. heterodoxum* var. *novomexicanum* in the ITS only (85% BS, 0.98 PP), *waxy* only (87% BS, 1.0 PP) and combined analyses (80% BS, 1.0 PP), and, along with *S. citrullifolium* var. *knoblichii*, comprises a monophyletic group in the *waxy* only (100% BS, 1.0 PP) and combined analyses (65% BS, 1.0 PP), here termed the Glandulosa clade.

Species- and Infraspecific-Level Monophyly—Species-level monophyly was examined in a number of taxa with multiple accessions sequenced in the phylogeny. In the cases of *S. rostratum*, *S. grayi*, *S. johnstonii*, *S. davisense*, *S. tribulosum*, and *S. tenuipes*, all accessions of the same species formed monophyletic groups with strong support in the combined trees. Furthermore, the multiple accessions sequenced of *S. citrullifolium* var. *citrullifolium* and *S. heterodoxum* var. *setigeroides* each emerged as monophyletic in all combined analyses, but *S. citrullifolium* var. *setigerum* is paraphyletic in the combined MP strict consensus tree. However, *S. citrullifolium*, *S. heterodoxum*, and *S. grayi* var. *grandiflorum* were not supported as monophyletic, as multiple accessions of these taxa did not group together in the combined analyses.

Constraint Analyses—Constraining all of Whalen's series to be monophyletic resulted in trees significantly different than the most parsimonious tree from the combined dataset (Templeton's test $p = 0.0001$). When constraining sers. *Androceras* and *Violaceifolium* individually, the trees were also significantly different than the most parsimonious tree from the combined dataset ($p = 0.0455$ and 0.0477, respectively). Trees constraining all of the yellow-flowered taxa (i.e. species of ser. *Androceras* minus *S. tribulosum*) to monophyly were not significantly different than nonconstrained trees (Templeton's test $p = 0.6608$).

Discussion

Sectional Relationships and Monophyly of Section Androceras—Despite the various hypotheses regarding the sister group to sect. *Androceras*, our data support previous molecular studies in finding sect. *Crinitum* as sister to sect. *Androceras* (Levin et al. 2006; Weese and Bohs 2007). These groups are morphologically distinctive and this relationship merits further study. *Solanum sisymbriifolium* is sister to a clade composed of sect. *Androceras* and sect. *Crinitum* despite the fact that *S. sisymbriifolium* and sect. *Androceras* share highly divided leaves and strongly accrescent calyces, characters not found in sect. *Crinitum*. Lester et al. (1990) also found the seeds of sects. *Androceras* and *Cryptocarpum*, to which *S. sisymbriifolium* belongs, to be remarkably similar. We were not able to sample other members of sect. *Cryptocarpum* but further sampling might possibly place this group sister to sect. *Androceras*.

All three data sets strongly support the monophyly of sect. *Androceras* as circumscribed by Whalen (1979a, 1984). This molecular evidence, combined with unique morphological traits found in the leaves, flowers, and fruits, its distinctive flavonoid chemistry, and geographical distribution, leave little doubt that *Solanum* sect. *Androceras* is a monophyletic group.

Character Evolution and Monophyly of Whalen's Series in sect. Androceras—Whalen's (1979a) three series within sect. *Androceras* were distinguished by trichome, flower, and seed morphology as well as flavonoid chemistry and geographical distribution (Table 1). Whalen (1979a) circumscribed these series as natural phyletic groups; however, they were not defined in strict monophyletic terms (see paraphyly of sers. *Androceras* and *Violaceiflorum* in Fig. 15 in Whalen 1979a). It is clear in examining his matrix of morphological characters (Table 6 and Fig. 15 in Whalen 1979a), that many are homoplasious or autapomorphic. Additionally, the assessment of ancestral and derived characters as well as coding of characters are based on the author's interpretations (see secondarily lost characters in Table 5 in Whalen 1979a) and could be differently interpreted by other taxonomists. Given this and the fact that our combined molecular dataset contains 340 parsimony informative characters, it is not surprising that the addition of the 14 characters from Whalen's (1979a) dataset does not change the topology or resolution of the phylogeny (results not shown). The few synapomorphic characters in Whalen's (1979a) character matrix show support for ser. *Pacificum*, the only one of the three series that emerges as a monophyletic group in our molecular trees. Characters unique to this series include white, deeply stellate corollas, radially wrinkled seeds, and a geographical center of distribution on the Pacific slope of the Sierra Madre Occidental on the west coast of Mexico. Apparently these characters arose once in the Pacificum clade, although confirmation of this awaits sampling of the third member of ser. *Pacificum*, *S. leucandrum*.

Neither ser. *Androceras* nor *Violaceifolium* is supported as monophyletic in the molecular analyses. These series were paraphyletic in Whalen's (1979a) cladistic analysis and the nonmolecular characters that supported these groups are likely convergent. For instance, ser. *Androceras* was characterized by Whalen (1979a) as having stellate or multangulate cauline hairs and yellow corollas, lacking flavonoid compounds found in the other two series, and a distribution centered in the central Mexican highlands around Mexico City. These characters are found in species of the Rostratum clade (Fig. 2), but also in *S. johnstonii*, which does not form a part of this clade. Conversely, Whalen (1979a) placed *S. tribulosum* into ser. *Androceras* despite its pale blue or white corollas. Support and resolution along the backbone of the tree obtained here is weak or lacking, precluding firm conclusions about character evolution in sect. *Androceras* based on the most parsimonious trees. However, constraining all three series each to be monophyletic as well as constraining the taxa of Whalen's sers. *Androceras* and *Violaceifolium* individually to be monophyletic resulted in trees significantly different than the most parsimonious trees from the combined dataset. This further indicates that these two series are likely nonmonophyletic and that the characters that Whalen proposed to diagnose them have evolved multiple times. On the other hand, when all yellow-flowered taxa (i.e. species of ser. *Androceras* minus *S. tribulosum*) were constrained to monophyly, the constrained trees were not significantly different than nonconstrained trees. Therefore, the hypothesis of a single origin of yellow corollas within sect. *Androceras* cannot be rejected.

According to Whalen (1979a), nine of the species of sect. *Androceras* are taprooted annual herbs with wide edaphic tolerances. *Solanum johnstonii*, *S. tenuipes*, and *S. tribulosum*, however, are calciphilic herbaceous perennials. Judging from their widely separated positions on the molecular trees, it appears that the latter traits evolved independently in the three species.

Biogeographical Relationships—Based on his interpretation of cladistic relationships in sect. *Androceras*, Whalen

(1970a) considered ser. *Androceras* to be plesiomorphic within the section, implying an origin for the section in the central Mexican highlands (Whalen 1970a, 1983). However, the molecular phylogenies place *S. tenuipes*, included in ser. *Violaceifolium* by Whalen (1970a), as sister to the remainder of sect. *Androceras* with good support (82% BS, 1.0 PP). *Solanum tenuipes* occurs in the northern Chihuahua Desert near the Texas-Mexico border, pointing to a more northerly origin for the section. In the BI trees, the Glandulosa clade is in turn sister to the remainder of the species (Fig. 2). Species of this clade are also found in the northern Chihuahua Desert and range into the southwestern U. S. A., consistent with a northern origin. However, this latter relationship is poorly supported and collapses in the MP strict consensus trees. Nonetheless, molecular evidence refutes Whalen's (1970a, 1983) hypothesis of a central to southern Mexican origin for sect. *Androceras*.

Clades Within sect. Androceras—Rostratum clade—The Rostratum clade contains *S. rostratum*, *S. fructo-tecto*, and *S. angustifolium*, three of the five species placed by Whalen (1970a) in ser. *Androceras*. *Solanum rostratum* is a widely introduced weed and is common in the central and western U. S. A., but Whalen (1970a) considered central Mexico to be its area of origin due to the high level of morphological variability in this region and because many of the sister taxa proposed by Whalen (1970a) occur there. Our phylogeny samples accessions from both the U. S. A. and Mexico and all form a strongly supported group. Combined with many morphological characters, there is little doubt that, although it is the most widespread species in the section, *S. rostratum* is a monophyletic and distinct species. The other members of the Rostratum clade have more restricted distributions. *S. fructo-tecto* is found in the vicinity of Mexico City and Ciudad Durango, and *S. angustifolium* is found from southern Mexico through Honduras. Although *S. fructo-tecto* is vegetatively similar to *S. rostratum*, Whalen did not encounter hybrids or collections intermediate between the two species in reproductive characteristics. Therefore, he states that the overlap in vegetative characteristics between the species probably represents natural variation. Whalen (1970a) considered *S. angustifolium* to be closely related to *S. rostratum* but also called it a bridging taxon between his sers. *Androceras* and *Violaceiflorum*. Our phylogeny indicates that, despite sharing trichome and flavonoid characters with species in Whalen's ser. *Violaceiflorum*, *S. angustifolium* is in fact closely related to *S. rostratum*.

Pacificum clade—The Pacificum clade is found in western Mexico along the Pacific slope of the Sierra Madre Occidental and inland in central Mexico. This clade comprises two of the three species placed by Whalen (1970a) in ser. *Pacificum*, *S. leucandrum*, the third, was not sampled. *Solanum grayi* has been divided into two varieties based on flower size. The small-flowered form is known as *S. grayi* var. *grayi*, whereas the large-flowered plants are segregated as var. *grandiflorum*. Our phylogeny sampled species from throughout the range of *S. grayi* and did not consistently separate these varieties. These varieties seem to have arisen from character displacement in areas where *S. grayi* occurs sympatrically with its purported sister species *S. humboltzianum*. Whalen (1978b) showed that *S. humboltzianum* and *S. grayi* have similar sized flowers over their distinctive ranges, but show strong character displacement where their ranges overlap in Sonora and northern Sinaloa, with the flowers of *S. grayi* much smaller there than in other parts of its range. *Solanum grayi* and *S. humboltzianum* were shown to successfully hybridize in experimental crosses, but Whalen (1978b, 1979a) posits mechanical isolation via character displacement of floral traits in areas where the two species overlap, indicating that in nature they would not share the same pollinators and would effectively be reproductively isolated. Although our phylogenetic data suggest that the varietal distinctions in *S. grayi* might not be warranted, additional sampling from this species is needed to examine this question. The final member of Whalen's ser. *Pacificum*, *S. leucandrum*, is a rarely collected species and thus material was not available for this study. It is endemic to western Puebla and is morphologically similar to *S. grayi*, thus would likely be included in the Pacificum clade.

Setigeroid clade—The Setigeroid clade is strongly supported in our phylogeny and contains *S. davisense*, *S. citrullifolium* vars. *citrullifolium* and *setigerum*, and *S. heterodoxum* var. *setigeroides*. These species all occur in the southwestern U. S. A. and the area along the Texas-Mexico border. Our phylogeny shows that *S. davisense* is closely related to *S. citrullifolium* var. *citrullifolium* (76% BS, 1.0 PP), a result supported by allozyme data from Whalen (1979b). *Solanum davisense* is distinct from the other species of the Setigeroid clade due a more erect habit, acutely lobed leaves, smaller flowers, and smooth unridged seeds as well as chemical differences (Whalen 1979a). Divergence of *S. davisense* and *S. citrullifolium* was likely due to the slight geographical separation of *S. davisense* at the margin of the range of *S. citrullifolium* var. *citrullifolium* (Whalen 1979a, 1979b). *Solanum citrullifolium* vars. *setigerum* and *citrullifolium* do not form a monophyletic group in either the MP or BI combined analysis. Monophyly of *S. citrullifolium* var. *setigerum* itself is not supported in the MP strict consensus tree, yet it receives strong support (1.0 PP) in the BI 50% majority rule tree. Therefore, it is unclear whether the two varieties should be recognized as taxonomically distinct entities. As indicated by the common varietal name *setiger-* (Latin for "bristly"), *S. citrullifolium* var. *setigerum* and *S. heterodoxum* var. *setigeroides* share morphological similarities and have also been found to have a history of hybridization (Whalen 1970a). This, combined with the phylogenetic relatedness of these taxa, warrants a more detailed taxonomic investigation of these species and varieties to determine the relationship and specific delimitations of members of the Setigeroid clade.

Glandulosa clade—The Glandulosa clade presents interesting taxonomic and biogeographic problems. This clade contains *S. citrullifolium* var. *knoblichii*, *S. heterodoxum* var. *novomexicanum* and an unidentified species here called "Elder 46" based on the collector and collection number. *Solanum citrullifolium* var. *knoblichii* morphologically resembles var. *citrullifolium* but is restricted to western Chihuahua state in Mexico. It has longer hairs and more spreading fruit pedicels than the other varieties of *S. citrullifolium* but, due to a lack of collections, other morphological differences are not apparent. It is distantly related to its conspecifics, which occur in the Setigeroid clade (see above), and deserves further collection and taxonomic study. *Solanum heterodoxum* var. *novomexicanum* was given specific status [as *Androcera novomexicana* (Bartlett) Wooten & Standl.] by Wooten and Standley (1913). Despite the large geographic separation between *S. heterodoxum* var. *heterodoxum* from the area around Mexico City and var. *novomexicanum* from New Mexico, Whalen (1970a) felt that these varieties resembled each other except for the more stellate corollas in the latter variety. The geographically close *S. heterodoxum* var. *setigeroides* occurs in adjacent areas of New Mexico, Arizona, and the Texas-Mexico border. This variety

is distinct morphologically, with densely prickly stems and much finer spines than the other varieties of *S. heterodoxum*. Given the distinct morphological traits and the phylogenetic distance between *S. heterodoxum* var. *novomexicanum* and the other varieties, the specific classification of Wooten and Standley (1913) should be reconsidered. The final member of this clade, "Elder 46," is a collection from Jeff Davis County, Texas. This specimen has previously been identified as *S. grayi* var. *grandiflorum*, *S. daviesae*, and *S. heterodoxum* but does not fit any of those species concepts. Whalen did not examine this specimen, and use of his key and comparison to specimens he annotated does not result in a satisfactory determination. Since it appears that many of the species in the section are restricted endemics, it is possible that this collection represents an undescribed species.

The three species in the Glandulosa clade share some morphological characteristics including a diminutive weedy annual habit, violet or occasionally white flowers, and simple, often glandular hairs. Whalen (1979a) notes that the flavonoid profile for *S. heterodoxum* var. *novomexicanum* is identical to that of var. *heterodoxum*, however, the other members of the Glandulosa clade have not been sampled. The species in the Glandulosa clade have geographic ranges that do not appear to overlap, with "Elder 46" occurring in Jeff Davis County, Texas, *S. heterodoxum* var. *novomexicanum* occurring in north central New Mexico, and *S. citrullifolium* var. *knoblichii* restricted to Chihuahua, Mexico. Further systematic study and field collections will help to clarify the number of distinct taxa represented within this clade.

Solanum johnstonii—The two accessions of *S. johnstonii* emerge as a monophyletic group. This species has a very restricted range in the Durango state of north-central Mexico and has often been identified as *S. rostratum*. However, Whalen (1979a) cites many morphological differences as well as reproductive isolation as evidence that *S. johnstonii* and *S. rostratum* are distinct species. Our phylogeny supports this separation, but there is little support for the relationship of *S. johnstonii* with any of the other clades within sect. *Androceras*.

Solanum tribulosum—*Solanum tribulosum* shares purple flower color with members of the Whalen's ser. *Violaceifolium*, but he placed it in ser. *Androceras* due to geographical distribution, chemical characteristics (notably a lack of 8-hydroxyflavonoids and various flavones that are found in ser. *Violaceifolium*) and morphological features such as stellate corollas and smooth seeds. Results from the combined analyses indicate that *S. tribulosum* is more closely related to the other purple-flowered taxa here placed in the Setigeroid clade than to the species of Whalen's ser. *Androceras*, which include *S. rostratum*, *S. fructo-tecto*, and *S. angustifolium* (Rostratum clade) as well as *S. johnstonii*.

Solanum heterodoxum var. *heterodoxum*—The position of *S. heterodoxum* var. *heterodoxum* within the section is unresolved and it is not placed with either of the other *S. heterodoxum* varieties. This isolated phylogenetic position mirrors its geographical disjunction: *Solanum heterodoxum* vars. *setigeroides* and *novomexicanum* occur in the southwestern U.S.A., and northern Mexico, whereas var. *heterodoxum* is greatly disjunct in central Mexico. *Solanum heterodoxum* var. *heterodoxum* has less prickly stems with much stouter prickles than those of var. *setigeroides* and flowers with much more interpetalar tissue than those of var. *novomexicanum*. These differences, along with the phylogenetic results, indicate that *S. heterodoxum* as currently defined is almost certainly not monophyletic.

Solanum tenuipes—The two varieties of *S. tenuipes* are placed together as a strongly supported monophyletic group sister to all the other taxa of sect. *Androceras*. This species is found along the Texas-Mexico border and is divided into var. *tenuipes* and var. *latisectum* based on geography, leaf dissection, and seed size. Whalen (1979a) notes intermediates between these varieties and our phylogeny gives only weak support to grouping the two accessions of var. *tenuipes* (69% BS, 0.80 PP). Whalen (1979a) considered *S. tenuipes* to be derived within the section, making the placement of *S. tenuipes* at the base of sect. *Androceras* unexpected and worthy of further investigation.

Acknowledgments. The authors thank the late Michael D. Whalen for his numerous studies of sect. *Androceras*; Mario Vallejo-Marin for use of his images; LL, NY, and TEX and the Botanical Garden at the Radboud University in Nijmegen, The Netherlands for help in obtaining Solanaceae material; and Anne Bruneau and two anonymous reviewers whose comments greatly improved this manuscript. This work was supported by NSF grant DEB-0316614 to LB.

Literature Cited

Barker, F. K. and F. M. Lurzom. 2002. The utility of the incongruence length difference test. *Systematic Biology* 51: 625–637.

Bohs, L. 2004. A chloroplast DNA phylogeny of *Solanum* section *Lasiocarpa*. *Systematic Botany* 29: 177–187.

Bohs, L. 2005. Major clades in *Solanum* based on *ndhF* sequence data. Pp. 27–49 in *A festschrift for William G. D'Arcy: the legacy of a taxonomist*, ed. R. C. Keating, V. C. Hollowell, and T. B. Croat. St. Louis: Missouri Botanical Garden Press.

Bohs, L. and R. G. Olmstead. 2001. A reassesment of *Normania* and *Triguera* (Solanaceae). *Plant Systematics and Evolution* 228: 33–48.

Bohs, L., T. Weese, N. Myers, V. Lefgren, N. Thomas, A. van Wagenen, and S. Stein. 2007. Zygomorphy and heterandry in *Solanum* in a phylogenetic context. *Acta Horticulturae* 745: 201–223.

Bowers, K. A. 1975. The pollination ecology of *Solanum rostratum* (Solanaceae). *American Journal of Botany* 62: 633–638.

Cummings, M. P., S. A. Handley, D. S. Myers, D. L. Reed, A. Rokas, and K. Winka. 2003. Comparing bootstrap and posterior probability values in the four-taxon case. *Systematic Biology* 52: 477–487.

Danert, S. 1970. Infragenerische Taxa der Gattung *Solanum* L. *Die Kulturpflanze* 18: 253–297.

Darlu, P. and G. Lecointre. 2002. When does the incongruence length difference test fail? *Molecular Biology and Evolution* 19: 432–437.

Dolphin, K., R. Belshaw, D. L. C. Orme, and D. L. J. Quicke. 2000. Noise and incongruence: interpreting results of the incongruence length difference test. *Molecular Phylogenetics and Evolution* 17: 401–406.

Dunal, M. F. 1813. *Histoire naturelle, médicale et économique des* Solanum. Montpellier: Renaud.

Dunal, M. F. 1852. Solanaceae. Pp. 1–690 in *Prodromus Systematis Naturalis Regni Vegetabilis*, ed. A. P. de Candolle. Paris: Sociorum Treuttel et Würtz.

Erixon, P., B. Svennblad, T. Britton, and B. Oxelman. 2003. Reliability of Bayesian posterior probabilities and bootstrap frequencies in phylogenetics. *Systematic Biology* 52: 665–673.

Farris, J. S., M. Källersjö, A. G. Kluge, and C. Bult. 1994. Testing significance of incongruence. *Cladistics* 10: 315–319.

Farris, J. S., M. Kallersjo, A. G. Kluge, and C. Bult. 1995. Constructing a significance test for incongruence. *Systematic Biology* 44: 570–572.

Felsenstein, J. 1985. Confidence limits on phylogenies: an approach using the bootstrap. *Evolution* 39: 783–791.

Frodin, D. G. 2004. History and concepts of big plant genera. *Taxon* 53: 753–776.

Goloboff, P., J. Farris, and K. Nixon. 2008. TNT, a free program for phylogenetic analysis. *Cladistics* 24: 774–786.

Harris, J. A. and O. M. Kuchs. 1902. Observations on the pollination of *Solanum rostratum* Dunal and *Cassia chamaecrista* L. *Kansas University Science Bulletin* 1: 15–41.

Huelsenbeck, J. P. and F. Ronquist. 2001. MRBAYES: Bayesian inference of phylogenetic trees. *Bioinformatics* 17: 754–755.

Jesson, L. K. and S. C. H. Barrett. 2002. Solving the puzzle of mirror-image flowers. *Nature* 417: 707.

Knapp, S. 2002. Tobacco to tomatoes: a phylogenetic perspective on fruit diversity in the Solanaceae. *Journal of Experimental Botany* 53: 2001–2022.

Knapp, S., L. Bohs, M. Nee, and D. M. Spooner. 2004. Solanaceae – a model for linking genomics with biodiversity. *Comparative and Functional Genomics* 5: 285–291.

Lester, R. N., J. Francisco-Ortega, and M. Al-Ani. 1999. Convergent evolution of heterandry (unequal stamens) in *Solanum*, proved by spermoderm SEM. Pp. 51–69 in *Solanaceae IV: advances in biology and utilization*, ed. M. Nee, D. E. Symon, R. N. Lester, and J. P. Jessop. Kew: Royal Botanic Gardens.

Levin, R. A., K. Watson, and L. Bohs. 2005. A four-gene study of evolutionary relationships in *Solanum* section *Acanthophora*. *American Journal of Botany* 92: 603–612.

Levin, R. A., N. R. Myers, and L. Bohs. 2006. Phylogenetic relationships among the "spiny solanums" (*Solanum* subgenus *Lepthostemonum*, Solanaceae). *American Journal of Botany* 93: 157–169.

Maddison, W. P. and D. R. Maddison. 2000. MacClade 4: analysis of phylogeny and character evolution. Sunderland: Sinauer Associates.

Marzell, H. 1927. *Illustrierte Flora von Mitteleuropa*. Jena: Weissdorn-Verl.

Miller, R. E., M. D. Rausher, and P. S. Manos. 1999. Phylogenetic systematics of *Ipomoea* (Convolvulaceae) based on ITS and *waxy*. *Systematic Botany* 24: 209–227.

Mueller, L. A., T. H. Solow, N. Taylor, B. Skwarecki, R. Buels, J. Binns, C. Lin, M. H. Wright, R. Ahrens, Y. Wang, E. V. Herbst, E. R. Keyder, N. Menda, D. Zamir, and S. D. Tanksley. 2005. The SOL Genomics Network. A comparative resource for Solanaceae biology and beyond. *Plant Physiology* 138: 1310–1317.

Nuttall, T. 1818. *The genera of North American plants, and a catalogue of the species, to the year 1817*. Philadelphia: printed for the author by D. Heartt.

Peralta, I. E. and D. M. Spooner. 2001. Granule-bound starch synthase (GBSSI) gene phylogeny of wild tomatoes (*Solanum* L. section *Lycopersicon* [Mill.] Wettst. subsection *Lycopersicon*). *American Journal of Botany* 88: 1888–1902.

Posada, D. and K. A. Crandall. 1998. MODELTEST: testing the model of DNA substitution. *Bioinformatics* 14: 817–818.

Prager, E. M. and A. C. Wilson. 1988. Ancient origin of lactalbumin from lysozyme: analysis of DNA and amino acid sequences. *Journal of Molecular Evolution* 27: 326–335.

Rambaut, A. 1996. *Se-Al: sequence alignment editor*. Available at http://evolve.zoo.ox.ac.uk/. Oxford, U. K.: Department of Zoology, University of Oxford.

Simmons, M. P., K. M. Pickett, and M. Miya. 2004. How meaningful are Bayesian support values? *Molecular Biology and Evolution* 21: 188–199.

Symon, D. E. 1984. A new form of *Solanum* fruit. *Journal of the Adelaide Botanical Gardens* 7: 123–126.

Swofford, D. L. 2002. PAUP*: phylogenetic analysis using parsimony (* and other methods), version 4.0b10. Sunderland: Sinauer Associates.

Taberlet, P., L. Gielly, G. Pautou, and J. Bouvet. 1991. Universal primers for amplification of three non-coding regions of chloroplast DNA. *Plant Molecular Biology* 17: 1105–1110.

Templeton, A. 1983. Phylogenetic inference from restriction endonuclease cleavage site maps with particular reference to the evolution of humans and the apes. *Evolution* 37: 221–224.

Todd, J. F. 1882. Flowers of *Solanum rostratum* and *Cassia chamaecrista*. *American Naturalist* 16: 281–287.

Vallejo-Marin, M., J. D. Thomson, and S. C. H. Barrett. 2009. Division of labor within flowers: heteranthery, a floral strategy to reconcile contrasting pollen fates. *Journal of Evolutionary Biology* 22: 828–839.

Walpers, W. G. 1844. Solanaceae. Pp. 5–126 in *Repertorium Botanices Systematicae*, ed. W. G. Walpers. Leipzig: Friderici Hofmeister.

Weese, T. L. and L. Bohs. 2007. A three gene phylogeny of the genus *Solanum* (Solanaceae). *Systematic Botany* 32: 445–463.

Whalen, M. D. 1978a. Foliar flavonoids of *Solanum* section *Androceras*: a systematic survey. *Systematic Botany* 3: 257–276.

Whalen, M. D. 1978b. Reproductive character displacement and floral diversity in *Solanum* section *Androceras*. *Systematic Botany* 3: 77–86.

Whalen, M. D. 1979a. Taxonomy of *Solanum* section *Androceras*. *Gentes Herbarum* 11: 359–426.

Whalen, M. D. 1979b. Allozyme variation and evolution in *Solanum* section *Androceras*. *Systematic Botany* 4: 203–222.

Whalen, M. D. 1983. Centers of diversity, sympatry, and historical biogeography in the tropical plant genus *Solanum*. *Biologist (Columbus, Ohio)* 65: 78–95.

Whalen, M. D. 1984. Conspectus of species groups in *Solanum* subgenus *Leptostemonum*. *Gentes Herbarum* 12: 179–282.

White, T. J., T. Bruns, S. Lee, and J. Taylor. 1990. Amplification and direct sequencing of fungal ribosomal RNA genes for phylogenetics. Pp. 315–322 in *PCR protocols: a guide to methods and applications*, ed. M. Innis, D. Gelfand, J. Sninsky, and T. White. San Diego: Academic Press.

Wiens, J. J. 1998. Combining data sets with different phylogenetic histories. *Systematic Biology* 47: 568–581.

Wooten, E. O. and P. C. Standley. 1913. *Androcera novomexicanum*. *Contributions from the United States Herbarium* 16: 170.

APPENDIX 1. Summary of species, collection location, vouchers, and GenBank accession numbers for taxa used in this study provided in the order ITS, *waxy*, and *trnT-F*. Asterisks indicate specimens identified by M. D. Whalen. NIJ – cultivated at Radboud University, Nijmegen, The Netherlands.

S. acerifolium Dunal - Costa Rica, *Bohs 2714* (UT); AY561261, AY562949, AY266149. ***S. augustifolium*** Mill. - Oaxaca, Mexico, *Whalen 2* (LL)*; GQ143645, GQ143677, GQ149729. ***S. bahamense*** L. - NIJ 944750187, *Bohs 2936* (UT); AY996487, AY996386, GQ149730. ***S. betaceum*** Cav. – Bolivia, *Bohs 2468* (UT); AF244713, AY996387, DQ180426. ***S. carolinense*** L. – U. S. A., *Cipollini s. n.* (UT); AY996491, AY996392, DQ180476. ***S. citrullifolium* var. *citrullifolium*** - Burnet Co., Texas, *Urbatsch 4834* (NY); GQ143647, GQ143679, GQ149732. NIJ 894750197, *Bohs 3452* (UT); GQ143646, GQ143678, GQ149731. ***S. citrullifolium* var. *knoblichii*** Whalen - Chihuahua, Mexico, *Lebgue 3266* (NY); GQ143648, GQ143680, GQ149733. ***S. citrullifolium* var. *setigerum*** Bartlett - Chihuahua, Mexico, *Whalen 363* (LL)*; GQ143650, GQ143682, GQ149735. Presidio Co., Texas, *Turner 24-245* (TEX), GQ143649, GQ143681, GQ149734. ***S. crinitum*** Lam. – Brazil, *Agra et al. 7028* (JPB); GQ143651, GQ143683, GQ149736. Guyana, *Stern 253* (UT); GQ143652, GQ143684, GQ149737. ***S. daviesense*** Whalen - North population Jeff Davis Co., Texas, *Board s. n.* (NY); GQ143654, GQ143686, GQ149739. South population Jeff Davis Co., Texas, *Whalen 216* (LL)*; GQ143653, GQ143685, GQ149738. ***S. "Elder 46"*** - Jeff Davis Co., Texas, *Elder 46* (TEX); GQ143655, GQ143687, GQ149740. ***S. eusifolium*** C. E. Schulz - Puerto Rico, *Bohs 2461* (UT), AY996506, AY996409, DQ180483. ***S. fructo-tecto*** Cav. - Distrito Federal, Mexico, *Ults 28607* (NY); GQ143656, GQ143688, GQ149741. ***S. grayi* var. *grandiflorum*** Whalen - Jalisco, Mexico, *Guadalupe Ayala #91-9* (TEX), GQ143658, GQ143691, GQ149743. Sinaloa, Mexico, *Vallejo-Marin 07s195* (MEX), GQ143659, GQ143690, GQ149744. Sinaloa, Mexico, *Whalen 190* (LL)*, GQ143657, GQ143689, GQ149742. ***S. grayi* var. *grayi*** - Sonora, Mexico, *Reina 99-469* (TEX), GQ143660, GQ143692, GQ149745. ***S. heterodoxum* var. *heterodoxum*** - San Luis Potosí, Mexico, *Fryxell 3810* (NY), GQ143661, GQ143693, GQ149746. ***S. heterodoxum* var. *novomexicanum*** Bartlett - San Miguel Co., New Mexico, *Whalen 224* (LL)*; GQ143662, GQ143694, GQ149747. ***S. heterodoxum* var. *setigeroides*** Whalen - Cantron Co., New Mexico, *Shelton 127* (NY), GQ143664, GQ143696, GQ149749. Cochise Co., Arizona, *McGill 6785* (TEX); GQ143663, GQ143695, GQ149748. Sonora, Mexico, *Minckley s. n.* (UT) : GQ143665, GQ143697, GQ149750. ***S. johnstonii*** Whalen - Coahuila, Mexico, *Villarreal 4404* (TEX); GQ143666, GQ143698, GQ149751. Durango, Mexico, *Villarreal 6246* (TEX); GQ143667, GQ143699, GQ149752. ***S. lumholtzianum*** Bartlett - Sonora, Mexico, *Reina 99-398* (TEX), GQ143668, GQ143700, GQ149753. ***S. tycocarpum*** A. St.-Hil. – Paraguay, *Bohs 3213* (UT), AY996525, AY996435, DQ812107. ***S. mitlense*** Dunal – Mexico, *Whalen & Velasco 825* (BH); AY996530, AY996442, DQ812108. ***S. myriacanthum*** Dunal - NIJ 814750043, *Cipollini 83* (UT), AY561267, AY562960, AY559240. ***S. rostratum*** Dunal - Boulder Co., Colorado (no voucher); AY996550, AY996463, DQ180489. NIJ 934750126, *Cipollini 173* (UT); GQ143670, GQ143702, GQ149755. Puebla, Mexico, *Cipollini 184* (UT); GQ143669, GQ143701, GQ149754. ***S. sendtnerianum*** Van Heurck & Müll. Arg. – Brazil, *Lepsch da Cunha & Wang 316* (MO); GQ143671, GQ143703, GQ149756. ***S. sisymbriifolium*** Lam. – Bolivia, *Cipollini 132* (UT); AY561271, AY562967, AY266235. ***S. tenuipes* var. *latisectum*** Whalen - Chihuahua, Mexico, *Whalen 72* (LL)*; GQ143672, GQ143705, GQ149757. ***S. tenuipes* var. *tenuipes*** - Brewster Co., Texas, *Whalen 218* (LL)*; GQ143673, GQ143706, GQ149758. Nuevo León, Mexico, *Hinton 22874* (TEX); GQ143674, GQ143704, GQ149759. ***S. tribulosum*** Schauer - Guanajuato, Mexico, *Ventura 8236* (TEX); GQ143675, GQ143707, GQ149760. Veracruz, Mexico, *Whalen 18* (LL)*. GQ143676, GQ143708, GQ149761. ***S. wrightii*** Benth. - Costa Rica, *Bohs 2445* (UT), GQ480731, GQ480733, GQ480732.

The second and final sample in this packet is from a document created in LaTeX. Note the following for Chapter 3, the previously published chapter:

- The Table of Contents lists all the first- and second-level subheadings in the previously published chapter, just as it does for the other unpublished chapters.
- In the Table of Contents, the subheadings of the previously published chapter are numbered with a local numbering scheme even though the subheadings are not numbered in the actual article. A local numbering scheme is one in which subheadings, tables, and/or figures are numbered with the chapter number and then consecutively within that chapter; for example, 3.2 would indicate a subheading, table, or figure from Chapter 3 and that the subhead, table, or figure was the second one in Chapter 3, thus 3.2.
- In the List of Tables, those tables in the previously published article are also given a local numbering scheme, just like the subheadings. When a List of Tables or List of Figures is used and/or required and there is a previously published article in the thesis or dissertation, a local numbering scheme for tables and figures must be used.
- The entries in the List of Tables match the first full sentence of the table titles in the previously published chapter word for word.
- The title of Chapter 3 is exactly the same as the published article's title.

- On the part-title page, there is a permission statement containing all pertinent information such as authors, article title, journal name, volume and page numbers where the article appeared.
- The page numbers for the dissertation appear in the top right corner; that is, the pages on which the previously published article has been inserted into the dissertation are still numbered consecutively with the rest of the dissertation pages.
- The article fits within the 1 ¼" side margins and 1" top and bottom margins.

CONTENTS

LIST OF TABLES

CHAPTER 3

REGIONAL CHARACTERIZATION OF LONGITUDINAL DT-MRI TO STUDY WHITE MATTER MATURATION OF THE EARLY DEVELOPING BRAIN

Reprinted with permission from N. Sadeghi, M. Prastawa, P.T. Fletcher, J. Wolff, J. H. Gilmore, and G. Gerig. "Regional characterization of longitudinal DT-MRI to study white matter maturation of the early developing brain." *NeuroImage*, vol. 68, pp. 236–247, 2013.

NeuroImage 68 (2013) 236–247

Contents lists available at SciVerse ScienceDirect

NeuroImage

journal homepage: www.elsevier.com/locate/ynimg

Regional characterization of longitudinal DT-MRI to study white matter maturation of the early developing brain

Neda Sadeghi [a,*], Marcel Prastawa [a], P. Thomas Fletcher [a], Jason Wolff [b], John H. Gilmore [c], Guido Gerig [a]

[a] Scientific Computing and Imaging Institute, University of Utah, Salt Lake City, UT 84112, USA
[b] Carolina Institute for Developmental Disabilities, University of North Carolina, Chapel Hill, NC 27599, USA
[c] Department of Psychiatry, University of North Carolina, Chapel Hill, NC 27599, USA

ARTICLE INFO

Article history:
Accepted 15 November 2012
Available online 9 December 2012

Keywords:
Longitudinal brain imaging
Early brain development
DTI
Nonlinear mixed effect modeling

ABSTRACT

The human brain undergoes rapid and dynamic development early in life. Assessment of brain growth patterns relevant to neurological disorders and disease requires a normative population model of growth and variability in order to evaluate deviation from typical development. In this paper, we focus on maturation of brain white matter as shown in diffusion tensor MRI (DT-MRI), measured by fractional anisotropy (FA), mean diffusivity (MD), as well as axial and radial diffusivities (AD, RD). We present a novel methodology to model temporal changes of white matter diffusion from longitudinal DT-MRI data taken at discrete time points. Our proposed framework combines nonlinear modeling of trajectories of individual subjects, population analysis, and testing for regional differences in growth pattern. We first perform deformable mapping of longitudinal DT-MRI of healthy infants imaged at birth, 1 year, and 2 years of age, into a common unbiased atlas. An existing template of labeled white matter regions is registered to this atlas to define anatomical regions of interest. Diffusivity properties of these regions, presented over time, serve as input to the longitudinal characterization of changes. We use non-linear mixed effect (NLME) modeling where temporal change is described by the Gompertz function. The Gompertz growth function uses intuitive parameters related to delay, rate of change, and expected asymptotic value; all descriptive measures which can answer clinical questions related to quantitative analysis of growth patterns. Results suggest that our proposed framework provides descriptive and quantitative information on growth trajectories that can be interpreted by clinicians using natural language terms that describe growth. Statistical analysis of regional differences between anatomical regions which are known to mature differently demonstrates the potential of the proposed method for quantitative assessment of brain growth and differences thereof. This will eventually lead to a prediction of white matter diffusion properties and associated cognitive development at later stages given imaging data at early stages.

© 2012 Elsevier Inc. All rights reserved.

Introduction

Improved understanding of typical brain development during infancy, an interval characterized by rapid sculpting, organization and vulnerability to exogenous influences, is of a great importance both for clinical and scientific research. Many neurobehavioral disorders have their origins during neurodevelopment (Gilmore et al., 2010; Huppi, 2008). Establishing a normative model of early brain development is a critical step to understanding the timing and potential mechanisms of atypical development and how intervention might alter such trajectories and improve developmental outcomes (Als et al., 2004; Marsh et al., 2008). Once normative models are available, they can inform research and practice concerning children at risk for neurodevelopmental disorders and may eventually lead to earlier and improved diagnosis and treatment. Longitudinal trajectory-based studies provide a better understanding of human brain development compared to cross-sectional studies (Karmiloff-Smith, 2010). In cross-sectional data, calculation of the average trajectory may not be representative for the growth patterns of individual subjects as this approach is inherently insensitive to individual developmental differences and cohort effects (Gogtay et al., 2004). Cross-sectional analysis might falsely report magnitude of changes over time or may fail to detect changes (Casey et al., 2005).

Growth modeling from longitudinal data, on the other hand, makes use of sets of individual temporal trajectories which results in significantly improved models of growth and growth variability, as longitudinal studies can differentiate between cohort and age effects (Diggle et al., 2002).

Previous imaging studies of early brain development have substantially contributed to our current understanding of brain development. Some of the studies considered size or shape differences (Huppi, 2008; Knickmeyer et al., 2008; Xu et al., 2008; Xue et al., 2007), others have looked at changes of contrast in MRI (Sadeghi et al., 2010) or

* Corresponding author.
E-mail address: neda@sci.utah.edu (N. Sadeghi).

1053-8119/$ – see front matter © 2012 Elsevier Inc. All rights reserved.
http://dx.doi.org/10.1016/j.neuroimage.2012.11.040

diffusion parameters in DTI (Gao et al., 2009; Geng et al., 2012; Hermoye et al., 2006; Huppi et al., 1998; Mukherjee et al., 2002; Sadeghi et al., 2012). However, most of these studies are based on cross-sectional data or children older than 2 years (Dubois et al., 2008; Faria et al., 2010; Gao et al., 2009; Hermoye et al., 2006; Mukherjee et al., 2002). In this study we focus on developing longitudinal models spanning birth to about two years of age. The models are based on the parameters obtained from diffusion tensor imaging (DTI). DTI-derived diffusivity parameters provide relevant information about the maturation of the underlying tissue as they assess water content (Huppi, 2008). These measurements are a possible reflection of axonal density and/or degree of myelination (Neil et al., 1998; Song et al., 2002) which correlate with cognitive functions (Dubois et al., 2006) and early developmental outcomes (Als et al., 2004; Ment et al., 2009; Wolff et al., 2012). In this study we focus on fractional anisotropy (FA), mean diffusivity (MD), radial (RD) and axial diffusivity (AD) to explain brain maturation and to gain a better understanding of white matter development. Driven by earlier findings that myelination follows a nonlinear spatio-temporal pattern (Dubois et al., 2008), our goal is to capture these changes in terms of the parameters of the Gompertz function which provides an intuitive parameterization representing delay, growth, and asymptotic values for each region.

In contrast to previous studies, we use an explicit growth function (the Gompertz function) and a nonlinear mixed effect modeling scheme (Pinheiro and Bates, 2000). In a nonlinear mixed effects model, the diffusion parameters are modeled in a hierarchical fashion, with fixed-effect representing the overall population trend, and random effect associated with each individual. Nonlinear mixed effect models are suited for longitudinal data where each subject has repeated scans with the possibility of missing data points and uneven spacing between scans of all the individuals in the group. Unlike most previous studies of early brain development, we make use of longitudinal imaging where each subject is imaged repeatedly over the first few years of life. This enables a more accurate characterization of developmental pattern (Giedd et al., 1999). Nonlinear mixed effect model provides a direct way of estimating individual trajectories along with longitudinally derived typical developmental curves as illustrated in Fig. 2. This leads to the characterization of a normative model for healthy developmental patterns and estimation of personalized, individual trajectories of growth, which is a property that will be desirable for comparison and diagnostic assessment of individual subjects.

We apply our analysis framework to a set of white mater regions that are known to have different patterns of growth to establish normative developmental patterns for each region. Quantitative analysis of diffusion changes in these regions provide further insight into brain maturation process and will enable prediction of subject-specific growth trajectory with the potential of detecting pathological deviation related to brain disorders.

Materials and methods

Subjects

This study was approved by the Institutional Review Board of the University of North Carolina School of Medicine. Children analyzed in this study are controls in an ongoing longitudinal study of early brain development in high risk children (Geng et al., 2012). A total of 26 control subjects were selected for this study. Scans of these subjects were obtained at around two weeks, 1 year and 2 years. Four of the subjects had sub-optimal scans at 1 year that were removed, but their scans for other time points were kept. In total, we used 59 datasets, the temporal distribution of scan data is shown in Table 1. To ensure maximal success rate of scanning, all subjects were fed, swaddled and fitted with ear protection. All subjects were scanned without sedation during their natural sleep.

Table 1
Distribution of scans across different time points, *N* indicates the number of subjects with the associated temporal pattern.

Available scans	N
Neonate scan only	2
1 year scan only	0
2 year scan only	0
Neonate + 1 year scan	10
Neonate + 2 year scan	2
1 year + 2 year scan	3
Neonate + 1 year + 2 year scan	9

Image acquisition and data processing

All images were acquired using a 3 T Allegra head-only MR system using a single shot echo-planar spin echo diffusion tensor imaging sequence with the following parameters: TR = 5200 ms, TE = 73 ms, slice thickness of 2 mm and in-plane resolution of 2×2 mm^2. One image without diffusion gradients ($b = 0$) along with 6 gradient directions with a b-value of 1000 mm^3/s were acquired. The sequence was repeated 5 times for improved single-to-noise ratio. All DWIs were checked and corrected for motion artifacts using the DTIChecker tool.[1] Tensor maps were calculated for each DTI scan using weighted least squares tensor estimation on the images that have been averaged over sequence repeats (Salvador et al., 2005). T2-weighted structural images were obtained using turbo spin echo sequence with TR = 7 s, TE = 15 and 90 ms, slice thickness of 1.95 mm and in-plane resolution of 1.25×1.25 mm^2. T2W and baseline DWI of all the subjects' scans were skull stripped using Brain Extraction Tool (BET) (Smith, 2002).

Due to significant contrast changes in early brain development, we utilized two registration frameworks: one for intra-subject and inter-modality registration, and the other for inter-subject registration. For inter-subject registration, we applied the unbiased atlas building framework of Joshi et al. (2004) based on the Large Deformation Diffeomorphic Metric Mapping (LDDMM) (Miller et al., 2002) to the set of T2W images of scans at year 1 to obtain spatial mappings between all subjects through the estimated atlas coordinate system. Intra-subject registration was performed by IRTK software, using affine and nonlinear registration method of Rueckert et al. (1999) using normalized mutual information as the image match metric (Studholme et al., 1999) that appears robust to changing contrast properties in early brain development.[2] All time points of each subject are registered to the unbiased atlas via linear and non-linear transformations, first by mapping these images to the year 1 scan and then cascading the two transformations for a mapping to the atlas. Details on the registration methods and parameters are summarized in Appendix A. The tensors are registered to the atlas using transformations obtained by registering the DTI baseline (B0) images to T2W images. Tensors are resampled using finite strain reorientation and Riemannian interpolation (Alexander et al., 2001; Fletcher and Joshi, 2007; Pennec et al., 2006). After all the images are transformed into the atlas space, the tensors are averaged using the log-Euclidean method to produce a tensor atlas (Arsigny et al., 2006). In this study, we extract the mean, axial, radial diffusivity, and fractional anisotropy features from the registered tensors, $MD = \frac{\lambda_1+\lambda_2+\lambda_3}{3}$, $AD = \lambda_1$, $RD = \frac{\lambda_2+\lambda_3}{2}$ and $FA = \sqrt{\frac{1}{2}}\frac{\sqrt{(\lambda_1-\lambda_2)^2+(\lambda_1-\lambda_3)^2+(\lambda_2-\lambda_3)^2}}{\sqrt{\lambda_1^2+\lambda_2^2+\lambda_3^2}}$ where λ_i are the eigenvalues of the tensor sorted from largest to smallest. Fig. 1 shows an overview of our method and analysis workflow.

Nonlinear mixed effects model

In this subsection, we describe the nonlinear mixed effects model used to analyze the longitudinal DTI data. Compared to a nonlinear

[1] http://www.ia.unc.edu/dev/download/dtichecker.
[2] http://www.doc.ic.ac.uk/~dr/software.

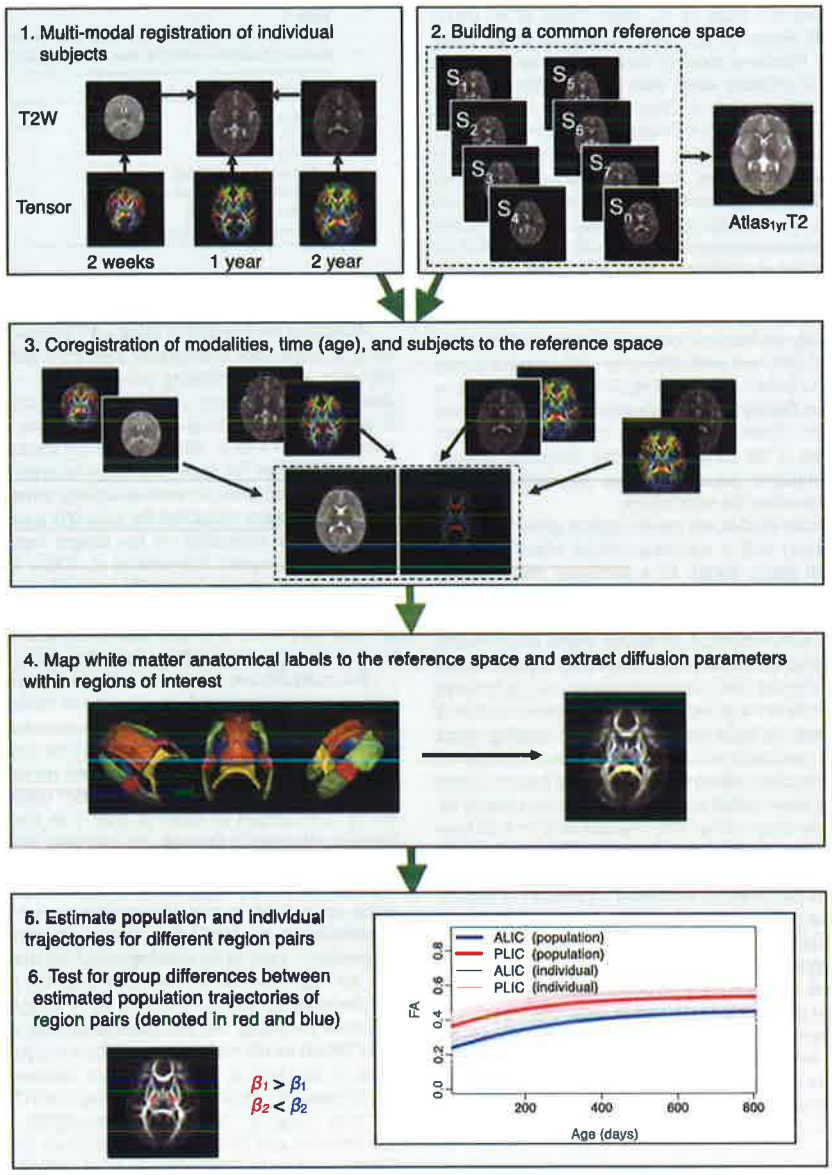

Fig. 1. Overview of the proposed longitudinal DTI region based analysis.

least squares (NLS) method, a nonlinear mixed effects (NLME) model does not assume that the sample data points are independent and identically distributed, rather it assumes that there is correlation across repeated measurements. Also, the average trend estimated based on the mixed effect model is an average of individual trajectories rather than a least squares fit to the individual data points. This results in better representation of trajectories in the population as illustrated in Fig. 2.

Model formulation

In the mixed effects model, the observed data is a combination of fixed effects which are parameters associated with the entire population or a sub-population, and random effects which are parameters associated to an individual. In the nonlinear mixed effect models, some or all the parameters appear nonlinearly in the model. We use the NLME model proposed by Lindstrom and Bates (1990) where each individual's observation is modeled as:

$$y_{ij} = f\left(\phi_i, t_{ij}\right) + e_{ij} \quad i = 1, \cdots, M; \quad j = 1, \cdots, n_i \tag{1}$$

where i indexes the individual subjects and j indexes the time points, M is the number of individuals, n_i is the number of observations on the ith individual, f is a nonlinear function of the covariate vector (time) t_{ij} and parameter vector ϕ_{ij}, and $e_{ij} \sim N(0,\sigma^2)$ is an i.i.d. error

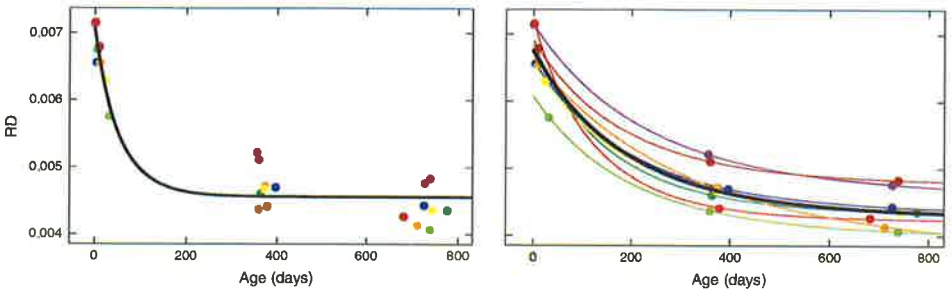

Fig. 2. Population growth models, represented as black curves, obtained using nonlinear least squares (NLS) in a cross-sectional fashion (left) and nonlinear mixed effect modeling (NLME) via longitudinal analysis (right). Colored points represent data observations, and colored curves represent the individual growth trajectories. Note that given the same data points, cross-sectional analysis provides a very different result than longitudinal analysis.

term. The parameter vector can vary among individuals by writing ϕ_i as

$$\phi_i = A_i\beta + B_i b_i \; b_i \sim N(0, \Psi) \tag{2}$$

where β is a p-vector of fixed effects, and b_i is a q-vector of random effects associated with individual i with variance–covariance Ψ. A_i and B_i are identity matrices for our study.

The function f can be any nonlinear function. Since early brain development is characterized by rapid initial development which slows down in later years, it is preferable to use growth functions which reflect these properties. One such growth function is the Gompertz function which can be written as:

$$y = \textbf{asymptote}\ \exp(-\textbf{delay}\ \exp(-\textbf{speed}\ t)). \tag{3}$$

The effects of varying the three parameters asymptote, delay and speed of the Gompertz function are shown in Fig. 3, for a function that decreases as time progresses.

To use the Gompertz function in the nonlinear mixed effect model, we apply the following formulation where the Gompertz function is parameterized as $y = f(\phi, t) = \phi_1 \exp\{-\phi_2\phi_3^t\}$, where ϕ_1 denotes asymptote, ϕ_2 is delay, and ϕ_3 is exp(−speed). Combining the nonlinear mixed effect model with the Gompertz function, each observation can be represented as follows:

$$y_{ij} = f\left(\phi_i, t_{ij}\right) + e_{ij} = \phi_{1i} \exp\left\{-\phi_{2i}\phi_{3i}^{t_{ij}}\right\} + e_{ij} \tag{4}$$

where the mixed effects are $\phi_i = [\phi_{1i}\ \phi_{2i}\ \phi_{3i}]^T = \beta + b_i$, the fixed effects are $\beta = [\beta_1\ \beta_2\ \beta_3]^T$, and the random effects for each subject i are $b_i = [b_{1i}\ b_{2i}\ 0]^T$. We set one of the random effects to zero to reduce the number of random effects in the model. As we only have a maximum of three time points per subject, including an additional random effect may cause the matrix Ψ to be rank-deficient (singular) and thus create problems in the estimation of the parameters.

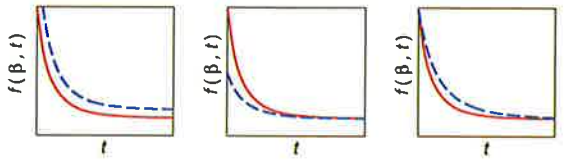

Fig. 3. Effect of varying the three parameters of the Gompertz function. The red curve shows the reference curve where parameters are held fixed. Left to right: the dashed blue curves show the effect of increasing values of β_1, β_2, and β_3 associated with asymptote, delay and speed, respectively.

Model estimation

Different methods have been proposed to estimate the parameters as shown in Eq. (4). Since random effects are unobserved quantities, we use the marginal density of responses y to obtain the parameters of the nonlinear mixed effects model. The following maximum likelihood estimation is performed to obtain the parameters of Eq. (4):

$$y_i : p\left(y_i|\beta, \Psi, \sigma^2\right) = \int p\left(y_i, |\beta, b_i, \Psi, \sigma^2\right) p(b_i) db_i. \tag{5}$$

Due to nonlinearity presented in the random effects of function f, there is generally no closed form solution to the integral. Here, we use the estimation method proposed by Lindstrom and Bates (1990) using the nlme package (Pinheiro et al., 2012) in R[3] to obtain the model parameters. This algorithm iterates between two steps: a penalized nonlinear least square step and a linear mixed effects step until convergence.

Inference and predictions

Under the linear mixed effects approximation, the distribution of maximum likelihood estimators $\hat{\beta}$ of the fixed effect is:

$$\hat{\beta} \sim N\left(\beta, \sigma^2\left[\sum_{i=1}^{M} \hat{X}\Sigma_i^{-1}\hat{X}_i\right]^{-1}\right) \tag{6}$$

where $\Sigma_i = I + \hat{Z}_i\Delta^{-1}\Delta^{-T}\hat{Z}_i^T$, $\hat{X}_i = \frac{\partial f_i}{\partial \beta^T}\big|_{\beta, b_i}$, $\hat{Z}_i = \frac{\partial f_i}{\partial b_i^T}\big|_{\beta, b_i}$, and Δ is the precision factor such that $\Psi^{-1} = \sigma^{-2}\Delta^T\Delta$ (Pinheiro and Bates, 2000).

Knowing fixed parameters $\hat{\beta}$ and its sampling distribution, it is straightforward to conduct hypothesis testing among different regions or between healthy and/or at-risk populations. We can also obtain individual growth trajectories based on the estimated random effects for each individual. For example, the individual response for subject i is $\hat{y}_i = f(\beta + b_i, t)$, and the population growth trajectory is estimated when random effects are set to their mean value, 0, resulting in $\hat{y} = f(\beta, t)$.

Regional analysis of longitudinal data using NLME

We use the nonlinear mixed effects to model the longitudinal DTI data within anatomical regions and perform hypothesis testing between trajectories of these regions. Maps of these anatomical regions were developed and disseminated by Mori et al. (2008), and mapped to our unbiased atlas via linear followed by nonlinear B-spline registration (Rueckert et al., 1999). We select 13 anatomical regions in the atlas space as shown in Fig. 4. In this study, left and right regions of anatomical locations are combined, giving a total of

[3] http://r-project.org.

eight regions. Future studies on lateralization of growth differences will analyze left and right regions separately. The labeling of regions in the atlas space allows automatic partitioning of each subjects' scans into the different anatomical regions. We then estimate growth trajectories for these regions using the NLME model (Lindstrom and Bates, 1990) described previously. The mixed parameters are the asymptote ϕ_1, delay ϕ_2 and speed ϕ_3 of the Gompertz function for each region, which requires a slight modification to Eq. (4) to account for regions:

$$y_{rij} = f\left(\phi_{ri}, t_{ij}\right) + e_{ij} = \phi_{1ri} \exp\left\{-\phi_{2ri}\phi_{3ri}{}^{t_{ij}}\right\} + e_{ij}. \quad (7)$$

We then conduct hypothesis testing between pairs of regions to determine modes of longitudinal changes in terms of the Gompertz growth parameters. With N number of regions, we perform $\frac{N(N-1)}{2}$ pairwise fitting of nonlinear mixed effect modeling. The significant parameters are determined through t-tests, corrected for multiple comparisons by Bonferroni correction. The parameters that are found to be significant between two pairs of regions can be interpreted as the distinguishing feature between the longitudinal trajectories of these regions.

Results

We applied our framework to longitudinal pediatric DTI data of 26 subjects. In total, we selected 13 regions in the unbiased atlas as shown in Fig. 4. The regions are as follows: anterior limb of internal capsule (right and left; ALIC), posterior limb of internal capsule (right and left; PLIC), genu, body of corpus callosum (BCC), splenium (Sp), external capsule (right and left; ExCap), retrolenticular part of internal capsule (right and left; RLIC), and posterior thalamic radiation which includes optic radiation (right and left; PTR). The right and left of each anatomical region were combined giving a total of eight regions. Fig. 5 plots the average FA, MD, RD, and AD of each region for each subject. In all the regions, FA increases with age, whereas MD, RD and AD decrease with age. Interestingly, each region develops in a distinctly different temporal pattern.

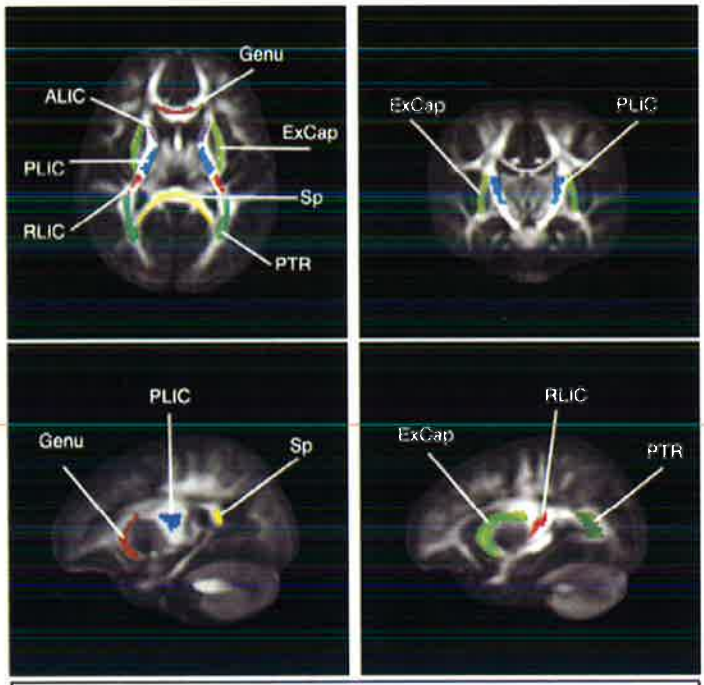

White matter anatomical structures	
Anterior limb of internal capsule	ALIC
Posterior limb of internal capsule	PLIC
Retrolenticular part of the internal capsule	RLIC
Posterior thalamic radiation	PTR
Genu of Corpus Callosum	Genu
Splenium of Corpus Callosum	Sp
Body of Corpus Callosum	BCC
External Capsule	ExCap

Fig. 4. White matter anatomical labels that are used for regional analysis. Labels are overlaid on the FA (Fractional Anisotropy) map of the reference space that is the population atlas.

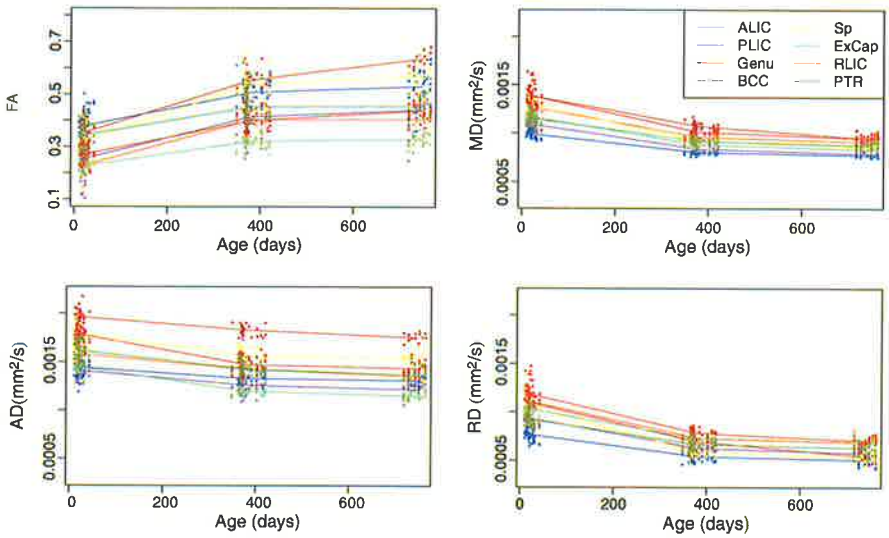

Fig. 5. Plots of diffusivity measures (FA, MD, AD and RD) versus age, shown for 26 control subjects and eight regions. Colors indicate different regions (purple: ALIC, light green: ExCap, brown: Genu, blue: PLIC, dark green: PTR, red: RLIC, yellow: Sp, orange: BCC), solid lines connect the mean of each region. In all the regions, FA increases with age, whereas MD, RD and AD decrease with age. Interestingly, each region develops in a distinctly different temporal pattern.

Paired t-tests of growth trajectories were performed for all combination of pairs of regions for all the diffusion parameters. The results of all pairwise comparisons can be found in Table 3 in Appendix B. Differences in parameters β_1 and β_2 were significant between most pairwise comparisons among diffusion parameters, whereas β_3 was only significant in a few regions: genu, splenium, and body of corpus callosum, and mostly when considering the RD or MD measurements. Genu was the only structure that was significantly different than all the other regions in the β_3 parameter of RD and MD. This region decreased in MD and RD at a slower rate compared to all the other regions. We didn't find any pattern that was consistent among different parameters and different measurements since each parameter measures a different aspect of growth. Interestingly, we noticed some pairwise comparisons with significant differences in β_1 parameter between AD and RD trajectories, but no differences in MD (ALIC vs. PLIC, Genu vs. ExCap). This happens when reverse temporal patterns are seen for AD and RD, suggesting that analysis of AD and RD may reveal much better insight into maturation than MD alone.

In this section, we focus on PLIC/ALIC, body of corpus callosum (BCC), and splenium comparisons as examples of commissural and projection fibers. These regions are known to have a distinctive maturation pattern and axonal density. The PLIC is one of the structures

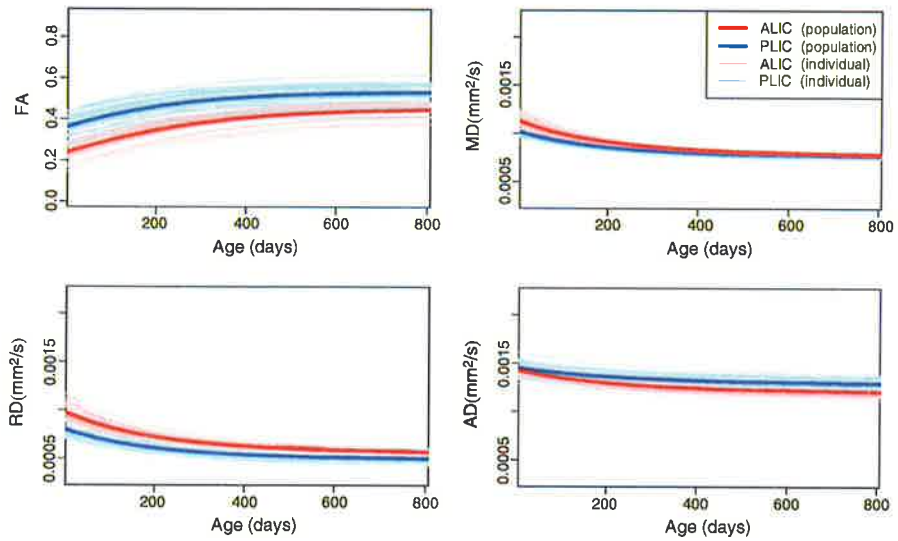

Fig. 6. Population and individual growth trajectories for PLIC and ALIC regions. Thicker curves illustrate the average growth trajectories, and individual trajectories are shown via the red and blue functions of individual subjects for ALIC and PLIC, respectively. Gompertz parameters with statistically significant differences are: FA: β_1^{**}, β_2^{**}, MD: β_2^{**}, RD: β_1^{**}, β_2^{**}, AD: β_1^{*}, where * denotes $p<0.05$, ** denotes $p<0.01$ and where β_1, β_2 and β_3 represent asymptote, delay and speed.

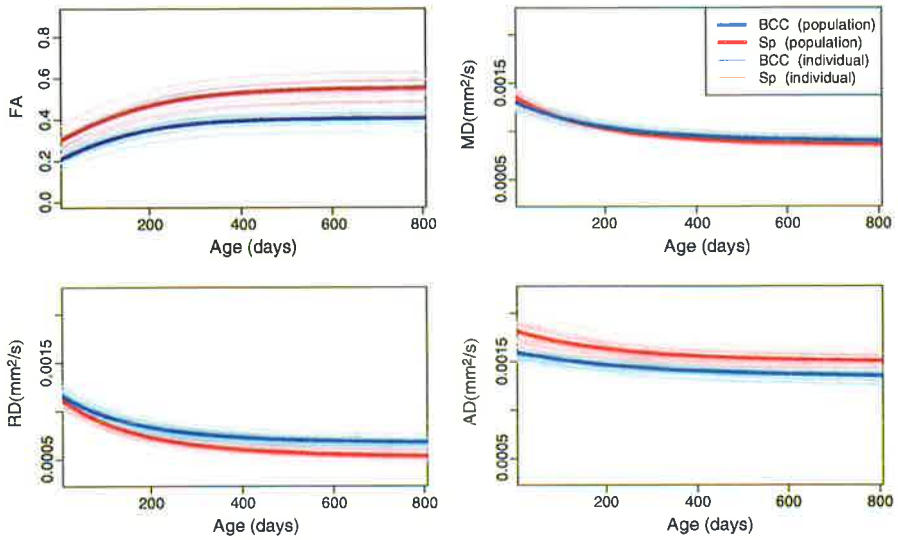

Fig. 7. Population and individual growth trajectories for the body of the corpus callosum (BCC, blue) and the splenium (Sp, red). Thick curves are the average growth trajectories. Gompertz parameters with significant differences are: FA: β_1^{**}, β_2^{**}, MD: β_2^{**}, RD: β_1^{**}, β_2^{**}, AD: β_1^{*}, where * denotes $p<0.05$, ** denotes $p<0.01$ and where β_1, β_2 and β_3 represent asymptote, delay and speed, respectively.

that shows early myelination, while ALIC shows later maturation compared to PLIC as is shown in higher FA, and lower RD and MD. Fig. 6 shows the population and individual trajectories of FA, MD, RD and AD as modeled by Nonlinear Mixed Effect for ALIC/PLIC. As expected, the PLIC shows a higher FA compared to ALIC at birth mainly explained by lower RD. After about 800 days both regions have the same MD and similar FA and RD values. However, the ALIC shows a higher AD compared to PLIC, possibly indicating a different structuring of this tract region. The delay parameter of the Gompertz function β_2 was significantly different between ALIC and PLIC for FA, MD, and RD measurements, an indication of later development of ALIC compared to PLIC. Also, the asymptote β_1 was significantly different for FA, RD and AD.

The body of the corpus callosum (BCC) and splenium (Sp) are known to have very limited myelination at birth but higher axonal density compared to ALIC and PLIC, and the splenium shows earlier myelination compared to BCC (Rutherford, 2002). Fig. 7 shows population and individual growth trajectories for the body of the corpus callosum and splenium. The splenium shows higher FA at birth and also throughout the first two years, while RD is about same at birth, but diverges at two years. Reverse patterns are seen for AD and RD at about two years, which causes MD to be about the same. All three parameters of the Gompertz function for RD were significantly different between BCC and Splenium, suggesting that RD may capture early maturation patterns more sensitively than the other measures. The asymptote parameter was significantly different among all the measurements between these two regions.

Fig. 8 shows FA, RD and AD of PLIC (shown in blue) compared to the other three regions ALIC, BCC, and Sp (shown in red). In this figure, solid lines are the average estimated growth trajectories for each region, the shaded regions are the 95% confidence interval of these average curves. Monte Carlo simulation was used to generate 1000 curves based on the approximate distribution of the maximum likelihood estimates of fixed effects. The 95% range of these curves are calculated pointwise to obtain the confidence interval. The dashed lines show the 95% predicted interval which is also calculated based on the Monte Carlo simulation of 1000 curves based on the approximate distribution of both fixed effects and random effects.

The splenium shows a high RD at birth relative to PLIC, by about 800 days however, both regions have approximately the same RD value as shown in Fig. 8. The splenium has very limited myelination at birth, while the PLIC is known to have a higher level of myelination at this time of development. These facts are evident in the difference in RD at birth between splenium and PLIC. At age two, however, the splenium shows approximately the same RD value, indicating that it catches up with PLIC.

The values of Gompertz parameters for all the regions and all diffusivity measures are shown in Fig. 9. Each region shows a distinct pattern of development as is depicted by the β_1, β_2, and β_3 parameters of Gompertz function. As indicated in the section 'Model formulation' the parameters β_1, β_2, and β_3 represent asymptote, delay and speed, respectively. When $\beta_1: R_A > R_B$, the expected value of diffusion parameters for region A is higher than region B at year 2. When $\beta_2: |R_A| > |R_B|$, region R_B matures earlier compared to R_A. The scenario $\beta_3: R_A > R_B$ indicates accelerated growth for R_B compared to R_A. Note that the delay parameter is negative for RD, AD and MD measurements as these values decrease during early brain development, where as the delay parameter is positive for FA as fractional anisotropy increases during this time period.

Discussion

Assessment of brain growth patterns in these regions reveals a nonlinear pattern of maturation with considerable regional variation as shown in previous studies (Hermoye et al., 2006; Mukherjee et al., 2001; Schneider et al., 2004). In agreement with previous studies, increased FA and decreased MD, AD, RD were observed within all the white matter regions during this period (Forbes et al., 2002; Mukherjee et al., 2001; Schneider et al., 2004; Zhang et al., 2005). This longitudinal pediatric study supports a rapid change during the first 12 month followed by slower maturation during the second year similar to previous studies (Geng et al., 2012; Hermoye et al., 2006). Our study, in addition to supporting earlier cross-sectional reports on negative correlation between age and diffusion parameters, provides greater statistical power to examine nonlinear pattern of maturation in various white matter regions.

Beyond the analysis of FA and MD measurements, in this study we included RD and AD analysis of these white matter regions. The regional comparisons of white matter regions indicates that

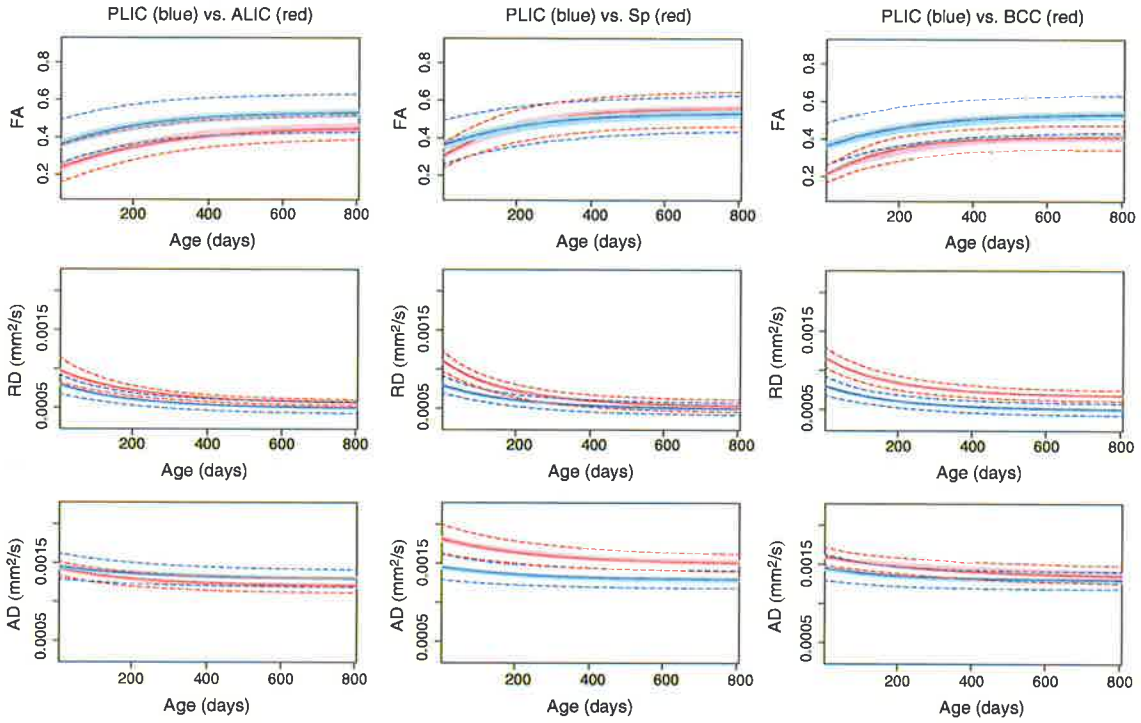

Fig. 8. PLIC (blue) compared to three other regions. Left column: ALIC (red), middle column splenium (red) and right column BCC (red). Solid curves are the estimated growth trajectories, the 95% confidence interval of the curves are shown as shaded regions. The dashed lines show the 95% predicted intervals for each region. Gompertz parameters with statistically significant differences are the following: ALIC vs. PLIC: FA: β_1^{**}, β_2^{**}, RD: β_1^{**}, β_2^{**}, AD: β_1^{*}. PLIC vs. Sp: FA: β_2^{**}, RD: β_2^{*}, AD: β_1^{**}, β_2^{*}. PLIC vs. BCC: FA: β_1^{**}, β_2^{**}, RD: β_1^{*}, where * denotes $p<0.05$, ** denotes $p<0.01$, and β_1, β_2 and β_3 represent asymptote, delay and speed, respectively.

individual AD and RD carry important information which may not be found in the MD diffusivity measures. The relationship of AD/RD and FA is complex and nonlinear, but our data suggest that modeling FA, AD, RD as time trajectories provides more information than only FA as illustrated in Figs. 6 and 7.

For example, FA of splenium and PLIC are approximately the same values at birth, yet we know that the splenium is not myelinated at birth, and we see the significant differences of RD between these regions. The high FA value of the splenium at birth may be due to its high density of axons. This discussion of FA for PLIC and splenium clearly reflects that FA is not necessarily a good indicator for the degree of myelination and may be greatly influenced by axonal density particular to this developmental interval (LaMantia and Rakic, 1990). In contrast, the similarity of FA trajectories for PLIC and splenium, for which we see very different AD and RD patterns and thus different tensor shapes, illustrates that interpretation of FA with respect to myelination and structural integrity is difficult, and that the additional AD and RD measures provide richer information.

Modeling the nonlinear growth changes of white matter by the Gompertz function and inclusion of AD and RD to the analysis provides a more detailed and comprehensive picture of the changes within these white matter regions. Compared to previous studies of linear fitting with logarithm of age (Chen et al., 2011; Faria et al., 2010; Lobel et al., 2009) we fit the nonlinear growth curves (Gompertz function) to the diffusion data and actual age, this enables the parameterization of the trajectories in terms of asymptote, delay and speed and models nonlinear temporal changes with improved accuracy. Based on our finding, the delay parameter of the Gompertz function, β_2 of RD seems to be closest related to myelination process if we compare results to what is known from the literature. Looking at RD and β_2 delay parameter of the Gompertz function as is shown in Fig. 9, we see a good correspondence with previous radiology findings, such as in Rutherford (2002). In fact, RD has been considered to be in correspondence with histological changes in demyelination (Song et al., 2002). Table 2 compares our findings versus existing knowledge from radiology literature, which indicates development of PLIC prior to ALIC, and splenium prior to genu which is also consistent with previous histological findings (Brody et al., 1987; Kinney et al., 1988).

Our framework is designed not only to provide qualitative comparisons, but to give researchers and clinicians quantitative parameters and a statistical testing scheme. Moreover, the method includes modeling of growth trajectories of individuals, resulting in personalized profiles. This property will be crucial for efforts to improve prediction and diagnosis for individuals, as well as partitioning groups of subjects according to subtypes and subtle variations in early developmental trajectories. Models which assume invariance or linearity between neurobehavioral markers are apt to miss crucial shifts in development (Shaw et al., 2006; Thomas et al., 2009). The ability of the present framework to capture the dynamic properties of inter- and intra-individual development has the potential to substantially improve clinical applications of developmental neuroimaging.

There are some limitations to our proposed framework. Our analysis depends on accurate image registration among all the subjects and time points. Early brain development is characterized by a rapid change of contrast and size of the brain, which makes registration a challenging task. However, in this study we decided to use ROI defined regions

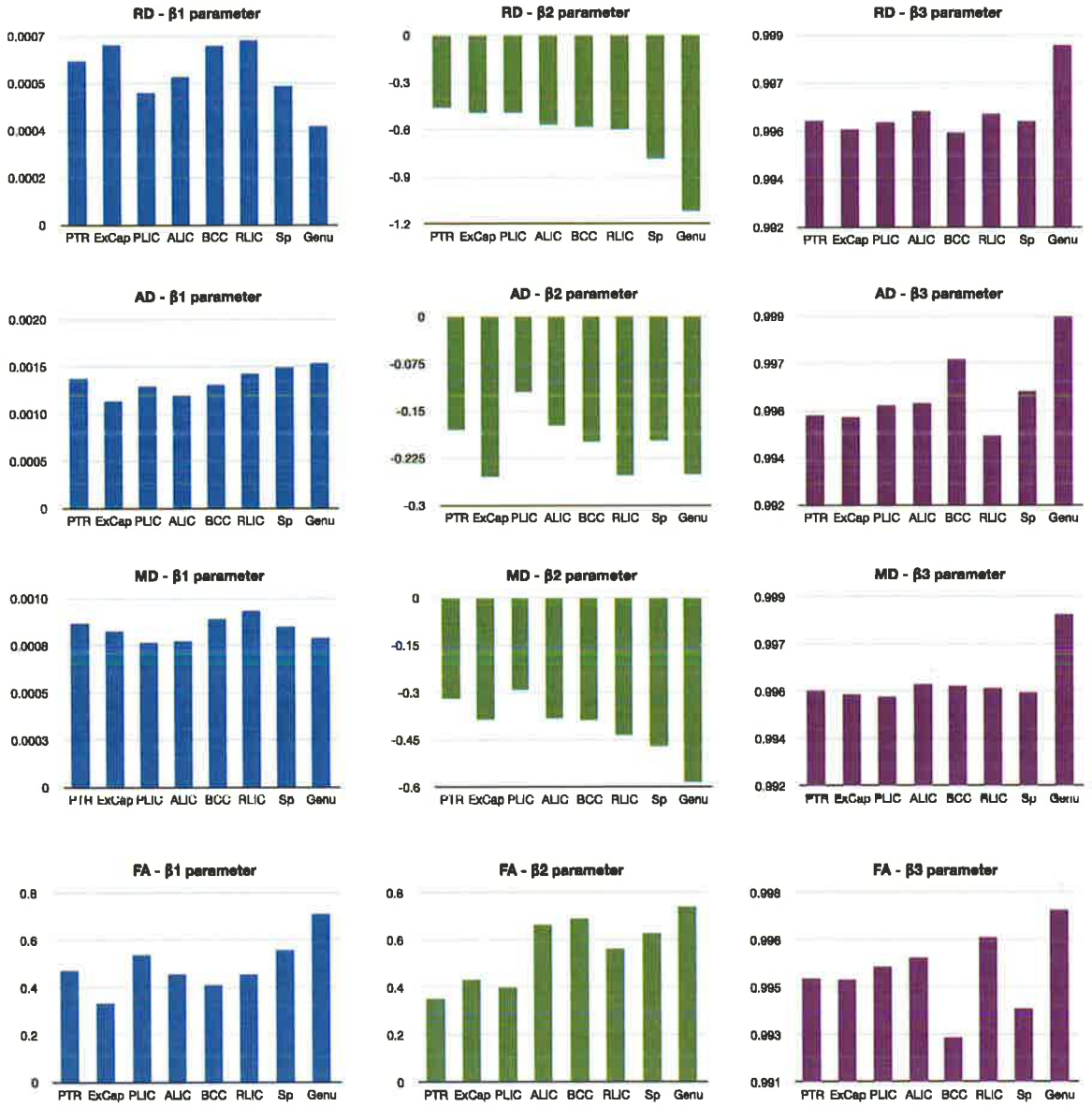

Fig. 9. Gompertz parameters RD, AD, MD and FA, from top to bottom. Left to right: β_1 is the asymptote parameter of the Gompertz function (blue), β_2 is the delay parameter (green), and β_3 is related to the speed (purple). The delay parameter is negative for RD, AD, and RD as the estimated model represents a decreasing Gompertz function, whereas the FA delay parameters are positive since FA values increase during development. When $\beta_1 : R_A > R_B$, the expected value of diffusion parameters for region A is higher than region B at year 2. When $\beta_2 : |R_A| > |R_B|$, region R_B matures earlier compared to R_A. $\beta_3 : R_A > R_B$ indicates accelerated growth for R_B compared to R_A.

Table 2
Relative order of appearance of myelin from term to 2 years.

Distribution of myelin as seen in T1W and T2W by Rutherforld	Estimated based on RD delay parameter β_2
PLIC and optic radiation	PLIC, PTR and ExCap
ALIC	ALIC and BCC
Not available	RLIC
Splenium	Splenium
Genu	Genu

which we expect to be more robust to misregistration compared to voxel-based analysis, and these regions are located more interiorly where we expect less registration problems. Nonetheless, improved spatial registration will potentially improve the accuracy of the model. Another limitation is that the statistical analysis is based on the log-likelihood of nonlinear mixed effects modeling, which does not have a closed form solution. We have used a linear mixed effect approximation, so greater care should be taken when doing hypothesis testing with the estimated parameters.

In the future, we plan to extend our method to tract-based regions with modeling along the tract changes. We also plan to extend the model to multivariate growth function similar to (Xu et al., 2008) and include a much larger set of regions for analysis.

Conclusions

We have presented a framework for the processing of longitudinal images in order to characterize longitudinal development of white matter regions at both the individual and group level. By utilizing nonlinear mixed effects modeling, we jointly estimate the population trajectory along with each individual trajectories. Gompertz parameterization of diffusion changes provides an intuitive parameterization of growth trajectory in terms of asymptote, delay and speed. This provides a description of longitudinal changes with potential for detecting deviations from a typical growth trajectory sensitive to multiple neurodevelopmental phenomena. We have also presented a method for making inference about regional differences in diffusion properties known to vary by microstructural properties and developmental course (Dubois et al., 2008; Kinney et al., 1988; LaMantia and Rakic, 1990; Lebel and Beaulieu, 2011). This is in contrast to standard modeling and analysis of testing for group or regional differences as it reveals the type, timing, and nature of differences. The proposed analysis can be extended to an arbitrary number of regions, and applied to other measurement such as structural MRI.

As discussed in the previous section, the present study clearly illustrate that studying FA alone as an indicator of white matter maturation or integrity insufficiently characterizes structural properties of white matter and may produce misleading results as regions with very different axonal density and differing degrees of myelination may show similar FA values. We suggest that in addition to FA, studies should include statistical analysis of AD and RD, which provide important additional information to better explain FA measures. In regard to early maturation, we demonstrate that the radial diffusivity (RD) measure and the delay parameter β_2 of the Gompertz function seem to be the best combination to describe early brain maturation. We will further explore this in applying our framework to DTI of infants with developmental delay and myelination storage disorders such as Krabbe's disease.

Acknowledgments

Supported by NIH grants: R01 MH070890 (JHG, GG), Conte Center MH064065 (JHG, GG), National Alliance for Medical Image Computing (NA-MIC) U54 EB005149 (GG) and the Utah Science Technology and Research (USTAR) initiative at the University of Utah.

Appendix A. Summary of registration parameters

Intra-subject and inter-modality registration

We use the IRTK software (Rueckert et al., 1999) to perform intra-subject and inter-modality registration. The registration method is a multi-scale approach using B-spline transformation, where we use the normalized mutual information image match metric. We use three different scales and discretize the image intensity histograms into 64 bins. In this study, the B-spline transforms are parametrized using $14\times14\times14$ control points.

Inter-subject registration

We construct an unbiased atlas (Joshi et al., 2004) and the associated inter-subject registration using the Large Deformation Diffeomorphic Metric Mapping (LDDMM) (Miller et al., 2002) that minimizes the following objective function:

$$\underset{v:\phi_t=v_t(\phi)}{\arg\min}\frac{1}{\sigma^2}\sum_i\left\|\bar{I}-I_i\circ\phi_i^{-1}\right\|_{L^2}^2+\sum_i\int_{t=0}^{T}\|v_{it}\|_V^2 \tag{8}$$

where $\bar{I}$ is the image atlas, I_i is the image of subject i, ϕ_i is the mapping relating subject i to the atlas that is parametrized using the velocity v_i. Regularity of the mapping ϕ is enforced by minimizing

$$\|v_t\|_V^2=\langle Lv,v\rangle, L=\alpha\nabla^2+\beta\nabla+\gamma I \tag{9}$$

Table 3
Results of pairwise testing of all white matter regions and all diffusivity measures. Gompertz parameters with significant differences are denoted by * for $p<.05$ and ** for $p<.01$. Non significant parameters are indicated by "ns".

		Alic	Plic	Genu	BCC	Sp	ExCap	Rlic	PTR
Alic	FA		β_1^{**}, β_2^{**}	β_1^{**}	β_1^{**}	β_1^{**}	β_1^{**}	ns	β_2^{**}
	MD	NA	β_2^{**}	β_2^{**}, β_3^{**}	β_1^{**}	β_1^{**}, β_2^{**}	β_1^{**}	β_1^{**}, β_2^{*}	β_1^{**}, β_2^{**}
	RD		β_1^{**}, β_2^{**}	β_1^{**}, β_2^{**}, β_3^{**}	β_1^{**}	β_2^{**}	β_1^{**}, β_2^{**}	β_1^{**}	β_1^{*}, β_2^{**}
	AD		β_1^{*}	ns	ns	β_1^{**}	β_1^{**}, β_2^{**}	β_1^{**}, β_2^{**}	β_1^{**}
Plic	FA	β_1^{**}, β_2^{**}		β_1^{**}, β_2^{**}	β_1^{**}, β_2^{**}	β_2^{**}	β_1^{**}	β_1^{*}, β_2^{*}	ns
	MD	β_2^{**}	NA	β_2^{**}, β_3^{**}	β_1^{**}, β_2^{**}	β_1^{**}, β_2^{**}	β_1^{**}, β_2^{**}	β_1^{**}, β_2^{**}	β_1^{**}
	RD	β_1^{**}, β_2^{**}		β_1^{*}, β_2^{**}, β_3^{**}	β_1^{*}	β_2^{**}	β_1^{*}	β_1^{**}, β_2^{**}	β_1^{**}
	AD	β_1^{*}		β_1^{**}, β_3^{**}	ns	β_1^{**}, β_2^{*}	β_1^{**}, β_2^{**}	β_1^{**}, β_2^{**}	ns
Genu	FA	β_1^{**}	β_1^{**}, β_2^{**}		β_1^{**},	β_1^{**}, β_2^{**}	β_1^{**}, β_2^{**}	β_1^{**}, β_2^{**}	β_1^{**}, β_2^{**}
	MD	β_2^{**}, β_3^{**}	β_2^{**}, β_3^{**}	NA	β_1^{**}, β_2^{**}	β_2^{**}	β_2^{**}, β_3^{**}	β_3^{**}	β_2^{**}, β_3^{**}
	RD	β_1^{**}, β_2^{**}, β_3^{**}	β_1^{**}, β_2^{**}, β_3^{**}		β_1^{*}, β_2^{**}, β_3^{**}	β_2^{**}	β_1^{**}, β_2^{**}, β_3^{**}	β_1^{**}, β_3^{**}	β_1^{**}, β_3^{**}
	AD	ns	β_1^{**}, β_3^{**}	ns		β_1^{**}	β_1^{**}, β_2^{**}, β_3^{**}	β_3^{**}	ns
BCC	FA	β_1^{**}	β_1^{**}, β_2^{**}	β_1^{**}		β_1^{**}	β_1^{**}, β_2^{**}	β_2^{*}	β_2^{**}
	MD	β_1^{**}	β_1^{**}, β_2^{**}	β_2^{**}, β_3^{**}	NA	β_1^{**}, β_2^{**}	β_1^{**}	ns	β_2^{**}
	RD	β_1^{**}	β_1^{*}	β_1^{**}, β_2^{**}, β_3^{**}		β_1^{**}, β_2^{**}, β_3^{**}	β_1^{*}	β_1^{**}, β_2^{**}, β_3^{**}	β_1^{**}, β_3^{**}
	AD	ns	ns	ns		β_1^{**}	β_1^{*}, β_2^{**}	ns	ns
Sp	FA	β_1^{**}	β_2^{**}	β_1^{**}, β_3^{**}	β_1^{**}		β_1^{**}, β_2^{**}	β_1^{**}	β_1^{*}, β_2^{**}
	MD	β_1^{**}, β_2^{**}	β_1^{**}, β_2^{**}	β_3^{**}	β_1^{**}, β_2^{**}	NA	β_1^{*}, β_2^{**}	β_1^{*}	β_2^{**}
	RD	β_2^{**}	β_2^{*}	β_3^{**}	β_1^{**}, β_2^{**}, β_3^{**}		β_1^{**}, β_2^{**}	β_1^{**}, β_2^{**}	β_1^{**}, β_2^{**}
	AD	β_1^{**}	β_1^{**}, β_2^{**}	β_1^{**}	β_1^{**}		β_1^{**}, β_2^{**}	ns	ns
ExCap	FA	β_1^{**}	β_1^{**}	β_1^{**}, β_2^{**}	β_1^{**}, β_2^{**}	β_1^{**}, β_2^{**}		β_1^{**}	β_1^{**}
	MD	β_1^{**}	β_1^{**}, β_2^{**}	β_2^{**}, β_3^{**}	β_1^{**}	β_1^{*}, β_2^{**}	NA	β_1^{**}	β_1^{*}, β_2^{**}
	RD	β_1^{**}, β_2^{**}	β_1^{**}	β_1^{**}, β_2^{**}, β_3^{**}	β_1^{**}	β_1^{**}, β_2^{**}		β_2^{**}	β_1^{**}
	AD	β_1^{**}, β_2^{**}	β_1^{**}, β_2^{**}	β_3^{**}	β_1^{**}, β_2^{**}	β_1^{**}, β_2^{**}		β_1^{*}	β_1^{**}, β_2^{**}
Rlic	FA	ns	β_1^{*}, β_2^{*}	β_1^{**}, β_2^{**}	β_2^{*}	β_1^{**}	β_1^{**}		β_2^{**}
	MD	β_1^{**}, β_2^{**}	β_1^{**}, β_2^{**}	β_3^{**}	ns	β_1^{*}	β_1^{**}	NA	β_1^{**}, β_2^{**}
	RD	β_1^{**}	β_1^{**}, β_2^{*}	β_1^{**}, β_3^{**}	β_1^{**}, β_2^{**}, β_3^{**}	β_1^{**}, β_2^{**}	β_2^{**}		β_1^{**}, β_2^{**}
	AD	β_1^{**}, β_2^{**}	β_1^{**}, β_2^{**}	β_3^{**}	ns	ns	β_1^{**}		β_2^{**}